3rd and 11th orders of accuracy of 'linear' and 'quadratic' elements for Poisson equation with irregular interfaces on Cartesian meshes

Received 2 September 2021
Revised 4 October 2021
4 November 2021
Accepted 8 November 2021

Alexander Idesman
Texas Tech University System, Lubbock, Texas, USA, and
Bikash Dey
University of Utah, Salt Lake City, Utah, USA

Abstract

Purpose – The purpose of this paper is as follows: to significantly reduce the computation time (by a factor of 1,000 and more) compared to known numerical techniques for real-world problems with complex interfaces; and to simplify the solution by using trivial unfitted Cartesian meshes (no need in complicated mesh generators for complex geometry).

Design/methodology/approach – This study extends the recently developed optimal local truncation error method (OLTEM) for the Poisson equation with constant coefficients to a much more general case of discontinuous coefficients that can be applied to domains with different material properties (e.g. different inclusions, multi-material structural components, etc.). This study develops OLTEM using compact 9-point and 25-point stencils that are similar to those for linear and quadratic finite elements. In contrast to finite elements and other known numerical techniques for interface problems with conformed and unfitted meshes, OLTEM with 9-point and 25-point stencils and unfitted Cartesian meshes provides the 3-rd and 11-th order of accuracy for irregular interfaces, respectively; i.e. a huge increase in accuracy by eight orders for the new 'quadratic' elements compared to known techniques at similar computational costs. There are no unknowns on interfaces between different materials; the structure of the global discrete system is the same for homogeneous and heterogeneous materials (the difference in the values of the stencil coefficients). The calculation of the unknown stencil coefficients is based on the minimization of the local truncation error of the stencil equations and yields the optimal order of accuracy of OLTEM at a given stencil width. The numerical results with irregular interfaces show that at the same number of degrees of freedom, OLTEM with the 9-points stencils is even more accurate than the 4-th order finite elements; OLTEM with the 25-points stencils is much more accurate than the 7-th order finite elements with much wider stencils and conformed meshes.

Findings – The significant increase in accuracy for OLTEM by one order for 'linear' elements and by 8 orders for 'quadratic' elements compared to that for known techniques. This will lead to a huge reduction in the computation time for the problems with complex irregular interfaces. The use of trivial unfitted Cartesian meshes significantly simplifies the solution and reduces the time for the data preparation (no need in complicated mesh generators for complex geometry).

The research of AI (theoretical developments) and BD (numerical study) has been supported in part by the Army Research Office (Grant Number W911NF-21–1-0267), the NSF grant CMMI-1935452 and by Texas Tech University. The views and conclusions contained in this paper are those of the authors and should not be interpreted as representing the official policies.

International Journal of Numerical Methods for Heat & Fluid Flow

0961-5539
DOI 10.1108/HFF-09-2021-0596

Originality/value – It has been never seen in the literature such a huge increase in accuracy for the proposed technique compared to existing methods. Due to a high accuracy, the proposed technique will allow the direct solution of multiscale problems without the scale separation.

Keywords Cartesian meshes, Poisson equation with discontinuous coefficients, Irregular interfaces, Local truncation error, Optimal accuracy

Paper type Research paper

1. Introduction

The Poisson equation for heterogeneous materials with interfaces is used for the description of many important phenomena such as heat transfer, multiphase flows, neurosciences and electrostatics. Therefore, many efforts are made for the development of accurate and computationally effective numerical techniques for this equation (Vallaghe and Papadopoulo, 2010; Crockett *et al.*, 2011; Zhang *et al.*, 2015; Guittet *et al.*, 2015; Coco and Russo, 2018; Gürkan and Massing, 2019; Zhang and Babuska, 2020; Guo and Lin, 2020; Li *et al.*, 2020; Xiao *et al.*, 2020). The finite element method, the finite volume method, the isogeometric elements, the spectral elements and similar techniques represent very powerful tools for the solution of partial differential equations (PDEs) for a complex geometry. However, for these techniques, it is difficult to control the quality of generated conformed meshes that may include 'bad' elements (e.g. elements with small angles). Such 'bad' elements lead to the degradation of accuracy. We should also mention that the discrete equations (e.g. based on the Galerkin approaches) of many numerical techniques do not provide the optimal accuracy. There is a significant number of publications related to the numerical solution of different PDEs on irregular domains with uniform embedded meshes. For example, we can mention the following fictitious domain numerical methods that use uniform embedded meshes: the embedded finite difference method, the cut finite element method, the finite cell method, the Cartesian grid method, the immersed interface method, the virtual boundary method, the embedded boundary method, etc. (Vos *et al.*, 2008; Burman and Hansbo, 2010; Rank *et al.*, 2011; Rank *et al.*, 2012; May and Berger, 2017; Main and Scovazzi, 2018; Song *et al.*, 2018; Kreisst and Petersson, 2006; Kreiss and Petersson, 2006; Kreiss *et al.*, 2004; McCorquodale *et al.*, 2001; Johansen and Colella, 1998). These techniques use unfitted meshes for irregular domains, the special treatment of small cut cells to avoid the degradation of accuracy and tend to achieve the accuracy close to that for the techniques with conformed meshes. A stable generalized finite element method for the Poisson equation was developed in Zhang and Babuska(2020) for heterogeneous materials with curved interfaces and unfitted uniform meshes. The second order of accuracy in the energy norm was achieved in Zhang and Babuska (2020) with two-dimensional quadratic finite elements that form 25-point stencils. The order of accuracy $p + 1$ for interface problems for the Poisson equation on unfitted meshes was reported in (Xiao *et al.*, 2020; Guo and Lin, 2019; Cheung *et al.*, 2020) for high-order immersed and extended finite elements of order p.

The development of robust numerical techniques for the solution of PDEs with complex irregular interfaces that provide an optimal and high order of accuracy is still a challenging problem.

Optimal local truncation error method (OLTEM) for the solution of PDEs with constant coefficients on regular and irregular domains with Cartesian meshes has been recently developed in our papers (Idesman, 2020; Dey and Idesman, 2020; Idesman and Dey, 2019; Idesman and Dey, 2020c; Idesman and Dey, 2020b; Idesman and Dey, 2020a; Idesman and Dey, 2020d). At the same structure of the semidiscrete or discrete equations, OLTEM provides the optimal order of accuracy that exceeds the order of accuracy of many known

numerical approaches on regular and irregular domains. For example, it was shown in Idesman and Dey (2020) that OLTEM with 25-point stencils for the two-dimensional Poisson equation with constant coefficients can provide the 18-th order of accuracy on regular domains. In our paper (Idesman and Dey, 2021), we have extended OLTEM with 9-point stencils (similar to those for linear finite elements) and unfitted Cartesian meshes to a much more general case of the two-dimensional time-dependent heat and wave equations with discontinuous coefficients and we have obtained the third order of accuracy of the new approach.

Here, we continue the development of OLTEM for heterogeneous materials with irregular interfaces started in our paper (Idesman and Dey, 2021) and we consider the development of OLTEM with 9-point and 25-point stencils (similar to those for linear and quadratic finite elements) and unfitted Cartesian meshes for the two-dimensional time-independent Poisson equation with discontinuous coefficients. Despite the different equations and the derivations compared to those in our paper (Idesman and Dey, 2021), the OLTEM with 9-point stencils also provides the third order of accuracy for the Poisson equation. OLTEM with 25-point stencils provides the 11-th order of accuracy for the Poisson equation with interfaces (i.e. the increase by 8 orders compared to known approaches for quadratic elements). We have never seen in the literature such a huge increase accuracy of numerical techniques for a general geometry of interfaces.

The Poisson equation in a composite domain $\Omega = \cup\Omega_l$ ($l = 1, 2, \ldots, \overline{N}$ where $\overline{N}$ is the total number of subdomains) can be written down in each subdomain Ω_l as follows:

$$e_l \nabla^2 u_l = f_l \,, \tag{1}$$

where e_l is a constant in each subdomain Ω_l and can be discontinuous across the interfaces between subdomains Ω_l ($l = 1, 2, \ldots, \overline{N}$), $f_l(\mathbf{x})$ is the source term that can be also discontinuous across the interfaces between subdomains Ω_l, u_l is the field variable. We also assume that the functions u_l and f_l are sufficiently smooth in each subdomain Ω_l. At the interface G between any two subdomains, the following interface conditions (the continuity of the function and the flux across the interface) are applied:

$$u_G^* - u_G^{**} = 0 \,, \qquad e_* \left(n_x \frac{\partial u_G^*}{\partial x} + n_y \frac{\partial u_G^*}{\partial y} \right) - e_{**} \left(n_x \frac{\partial u_G^{**}}{\partial x} + n_y \frac{\partial u_G^{**}}{\partial y} \right) = 0 \,, \tag{2}$$

where n_x and n_y are the x and y-components of the normal vector at the interface, e_* (e_{**}) is the corresponding material constant, the symbols * and ** correspond to the quantities on the opposite sides from the interface for the corresponding subdomains Ω_l. This means that the functions u_l are continuous across the interfaces but can have the discontinuous spatial derivatives across the interfaces.

Remark 1. The derivations for the new approach can be easily extended to the case with the discontinuous functions and fluxes across interfaces; i.e. when the right-hand sides in equation (2) are the given functions. However, for simplicity, we consider equation (2) with zero right-hand sides.

In this paper, the Dirichlet boundary conditions $u = g_1$ are applied along the boundary Γ where g_1 is the given function. However, the Neumann boundary conditions can be also used with the proposed approach (Idesman and Dey, 2020e; Idesman and Dey, 2020a). According to OLTEM, the discrete system for the Poisson equation after the space discretization with a Cartesian rectangular mesh can be represented as a system of algebraic equations. The

algebraic equation of this system for each internal grid point of the domain is called the stencil equation and can be written down for the case without interfaces as follows:

$$\sum_{i=1}^{M} k_i u_i^{num} = \overline{f}\,, \tag{3}$$

where u_i^{num} is the numerical solution for function u_i at the grid points, k_i are the unknown stencil coefficients to be determined, $\overline{f}$ is the discretized source term (Sections 2), M is the number of the grid points included into the stencil equation. Many numerical techniques such as the finite difference method, the finite element method, the finite volume method, the isogeometric elements, the spectral elements, different meshless methods and others can be finally reduced to equation (3) with some specific coefficients k_i. In the derivations below, we will assume 9-point ($M = 9$) and 25-point ($M = 25$) stencils in the two-dimensional case that are similar to 9-point and 25-point stencils of the two-dimensional linear and quadratic quadrilateral finite elements on Cartesian meshes, respectively. Generally, the stencils with any number of points M can be used with the suggested approach.

Let us introduce the local truncation error used with OLTEM. The replacement of the numerical values of function u_i^{num} at the grid points in equation (3) by the exact solution u_i to the Poisson equation, equation (1), leads to the residual e of this equation called the local truncation error of the discrete equation, equation (3):

$$e = \sum_{i=1}^{M} k_i u_i - \overline{f}\,. \tag{4}$$

Calculating the difference between equations (4) and (3) we can get:

$$e = \sum_{i=1}^{M} k_i \left[u_i - u_i^{num}\right] = \sum_{i=1}^{M} k_i \overline{e}_i^{u}\,, \tag{5}$$

where $\overline{e}_i^{u} = u_i - u_i^{num}$ are the errors of function u_i at the grid points i. As can be seen from equation (5), the local truncation error e is a linear combination of the errors of the function u at the grid points i which are included into the stencil equation.

In Section 2.1, OLTEM with 9-point and 25-point stencils is derived for the two-dimensional Poisson equation with discontinuous coefficients and zero source term. Its extension to nonzero source term is considered in Section 2.2. Two-dimensional numerical examples with the different shapes of interfaces, as well as the comparison with FEM are presented in Section 3. For the derivation of many analytical expressions presented below we use the computational program "Mathematica."

2. Optimal local truncation error method for the two-dimensional Poisson equation with discontinuous coefficients

2.1 Zero source term $f_l = 0$ in equation (1)

Let us consider a two-dimensional bounded domain and a Cartesian rectangular mesh with a mesh size h where h is the size of the mesh along the x–axis, $b_y h$ is the size of the mesh along the y–axis (b_y is the aspect ratio of the mesh). To simplify derivations, below we consider regular rectangular domains with irregular interfaces between different materials. However, irregular domains can be also considered with OLTEM (Idesman, 2020; Dey and Idesman, 2020; Idesman and Dey, 2019). In the paper, we will consider two different stencils used for

all internal grid points: 9-point uniform stencils that provide the third order of accuracy and 25-point uniform stencils that provide the 11-th order of accuracy. We should mention that we use the same structure of stencils for homogeneous and composite materials (the difference between homogeneous and composite materials is in the values of the stencil coefficients only).

The spatial locations of the 8 degrees of freedom that are close to the internal degree of freedom u_5 and contribute to the 9-point stencil for this degree of freedom are shown in Figure 1. The spatial locations of the 24 degrees of freedom that are close to the internal degree of freedom u_{13} and contribute to the 25-point stencil for this degree of freedom are shown in Figure 2. For convenience, the local numerations of the grid points from 1 to 9 and from 1 to 25 are used in Figures 1 and 2, as well as in the derivations below.

The interface in Figures 1(b) and 2(b) divides the 9-point or 25-point uniform stencil into two parts with different material properties. To impose the interface condition at the interface, we select a small number of interface points as follows. First we select one point at the interface with the coordinates $x_G = x_{G,1}$ and $y_G = y_{G,1}$. This point can be selected as the

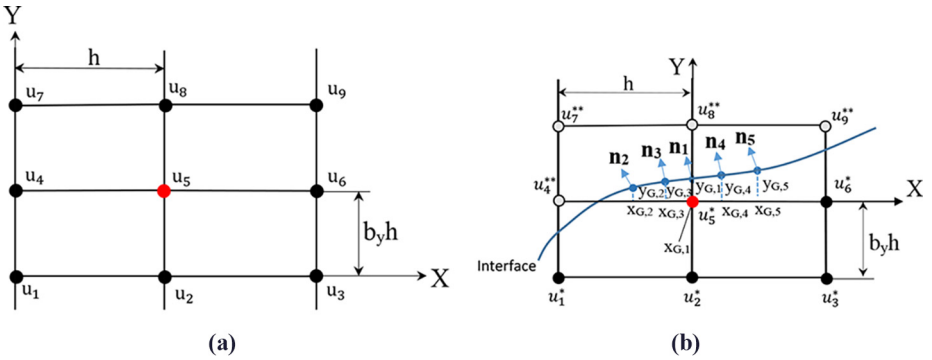

Figure 1.
The spatial locations of the degrees of freedom u_p ($p = 1, 2, \ldots, 9$) that contribute to the 9-point uniform stencil for the internal degree of freedom u_5 for homogeneous material without interface (a) and for heterogeneous material with interface (b)

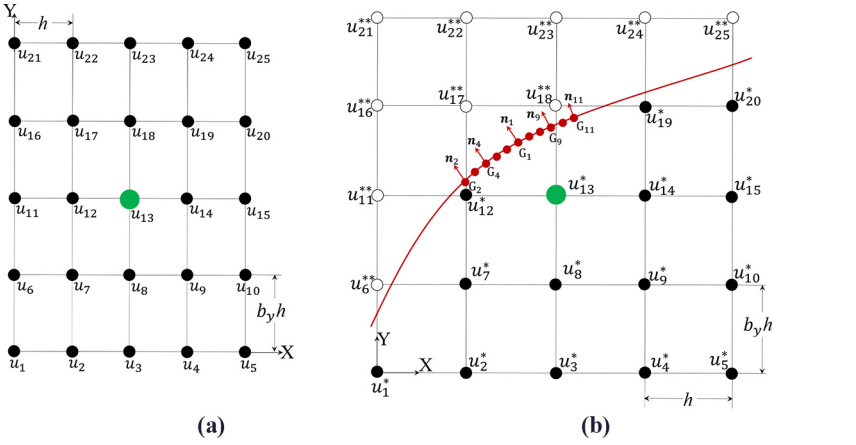

Figure 2.
The spatial locations of the degrees of freedom u_p ($p = 1, 2, \ldots, 25$) that contribute to the 25-point uniform stencil for the internal degree of freedom u_{13} for homogeneous material without interface (a) and for heterogeneous material with interface (b)

shortest distance from the internal grid point u_5 for the 9-point stencil or u_{13} for the 25-point stencil to the interface. Then, we additionally select n interface points to the left and to the right from the point with the coordinates $x_{G,1}$ and $y_{G,1}$ at the same distances $\overline{h} = \sqrt{(x_{G,i+1} - x_{G,i})^2 + (y_{G,i+1} - y_{G,i})^2}$ (i = 1,2,. . .,2n) from each other [Figures 1(b) and 2(b)]. The numerical experiments show that small distances $\overline{h} = h/10$ yield accurate results. The total number of interface points used is $N_G = 2n + 1$ where $N_G = 5$ for the 9-point stencils and $N_G = 11$ for the 25-point stencils [Figures 1(b) and 2(b)].

Let us describe the coordinates of the grid points of the 9-point and 25 point uniform stencils (Figures 1 and 2) with respect to their central point u_5 for the 9-point stencils and u_{13} for the 25-point stencils as follow:

$$x_p = x_5 + (i-2)h\,, \qquad y_p = y_5 + (j-2)b_y h\,, \tag{6}$$

for the 9-point stencils where $p = 3(j-1) + i$ with $i, j = 1, 2, 3$ and:

$$x_p = x_{13} + (i-3)h\,, \qquad y_p = y_{13} + (j-3)b_y h\,, \tag{7}$$

for the 25-point stencils where $p = 5(j-1) + i$ with i, j = 1,2,3,4,5.

To describe the coordinates of the selected N_G points on the interface [Figures 1(b) and 2(b)] we introduce $2N_G$ coefficients $d_{x,p}$ and $d_{y,p}$ ($p = 1, 2, \ldots, N_G$) with $N_G = 5$ for the 9-point stencils and $N_G = 11$ for the 25-point stencils as follows [Figures 1(b) and 2(b)]:

$$x_{G,j} = x_G + d_{x,j}h\,, \qquad y_{G,j} = y_G + d_{y,j}b_y h\,, \qquad j = 1, 2, \ldots, N_G\,. \tag{8}$$

where $d_{x,1} = d_{y,1} = 0$ for the central interface point $G = G_1$ with the coordinates $x_G = x_{G,1}$ and $y_G = y_{G,1}$ [Figures 1(b) and 2(b)].

Remark 2. Some of the interface points G_i (i = 1, 2, . . ., N_G) can be located slightly outside the 9-point or 25-point cells. The derivations presented below are also valid for these cases.

The stencil equation [equation (3)] for composite materials with the 9-point (Figure 1) or 25-point (Figure 2) uniform stencil for the grid point u_5 (for the 9-point stencils) or u_{13} (for the 25-point stencils) will be assumed in the following form:

$$\sum_{p=1}^{M} k_p \left[a_p u_p^{*,num} + (1 - a_p) u_p^{**,num} \right] = \overline{f}\,, \tag{9}$$

where $\overline{f} = 0$ in the case of zero source $f_l = 0$ in equation (1), $M = 9$ for the 9-point stencils and $M = 25$ for the 25-point stencils, the unknown stencil coefficients k_p (p = 1, 2, . . .,M) are to be determined from the minimization of the local truncation error, the coefficients $a_p = 1$ if the grid point u_p belongs to material * or $a_p = 0$ if the grid point u_p belongs to another material ** (i.e. only one variable $u_p^{*,num}$ or $u_p^{**,num}$ is actually included into equation (9) for each grid point; e.g. the coefficients a_p for Figure 1(b) are: $a_1 = a_2 = a_3 = a_5 = a_6 = 1$ and $a_4 = a_7 = a_8 = a_9 = 0$). The local truncation error e follows from equation (9) by the replacement of the numerical solution $u_p^{*,num}$ and $u_p^{**,num}$ by the exact solution u_p^* and u_p^{**}:

$$e = \sum_{p=1}^{M} k_p \left[a_p u_p^{*} + (1 - a_p) u_p^{**} \right] - \overline{f}\,. \tag{10}$$

One of the ideas of the new approach is to include the interface conditions for the exact solution at a small number N_G of the interface points in the expression for the local truncation error in equation (10) as follows:

$$e = \sum_{p=1}^{M} k_p \left[a_p u_p^* + (1 - a_p) u_p^{**} \right] + \left\{ \sum_{j=1}^{N_G} q_{1,j} \left(u_{G,j}^* - u_{G,j}^{**} \right) + \sum_{j=1}^{N_G} h q_{2,j} \left[e_* \left(n_{x,j} \frac{\partial u_{G,j}^*}{\partial x} + n_{y,j} \frac{\partial u_{G,j}^*}{\partial y} \right) - e_{**} \left(n_{x,j} \frac{\partial u_{G,j}^{**}}{\partial x} + n_{y,j} \frac{\partial u_{G,j}^{**}}{\partial y} \right) \right] \right\} - \bar{f}\,, \tag{11}$$

where $n_{x,j}$ and $n_{y,j}$ are the x and y-components of the normal vectors at the N_G selected interface points [Figures 1(b) and 2(b)], the coefficients $q_{1,j}$ and $q_{2,j}$ ($j = 1, 2, \ldots, N_G$) will be used for the minimization of the local truncation error in equation (11) (see Section 2.1.2 below), the expressions in parenthesis after $q_{1,j}$ and $q_{2,j}$ are the interface conditions at the N_G selected interface points. Therefore, the expression in the curled brackets in equation (11) is zero [equation (2)] and equations (10) and (11) yield the same local truncation error e. The addition of the interface conditions at N_G points in equation (11) with the unknown coefficients $q_{1,j}$, $q_{2,j}$ (j = 1,2,...,N_G) allows us to obtain the analytical expressions for the stencil coefficients for the horizontal interface, as well as to get a high accuracy for general geometry of interfaces.

Remark 3. Only $M + 2N_G - 1$ out of the $M + 2N_G$ coefficients k_p, $q_{1,j}$, $q_{2,j}$ ($p = 1, 2, \ldots, M$, $j = 1, 2, \ldots, N_G$) in equation (11) can be considered as unknown coefficients. This can be explained as follows. In the case of zero source $f_l = 0$ and $\bar{f} = 0$, equation (9) can be rescaled by the division of the left- and right-hand sides of equation (9) by any scalar; i.e. one of the coefficients k_p can be selected as unity and there will be only $M + 2N_G - 1$ unknown rescaled coefficients. The case of nonzero load $\bar{f} \neq 0$ can be similarly treated because the term $\bar{f}$ is a linear function of the stencil coefficients. For convenience, we will scale the stencil coefficients in such a way that k_m is $k_m = 1$ where $m = 5$ for the 9-point stencils and $m = 13$ for the 25-point stencils.

To represent the local truncation error e as a Taylor series, let us expand the exact solution at the grid points and the N_G selected interface points in equation (11) into a Taylor series at small $h \ll 1$ in the vicinity of the central interface point G for the 9-point stencils and 25-point stencils as follows:

$$\begin{aligned} v_p = v_G + \frac{\partial v_G}{\partial x}\left[((i-2) - dx_G)h\right] + \frac{\partial v_G}{\partial y}\left[((l-2) - dy_G)b_y h\right] \\ + \frac{\partial^2 v_G}{\partial x^2}\frac{\left[((i-2) - dx_G)h\right]^2}{2!} + \frac{\partial^2 v_G}{\partial y^2}\frac{\left[((l-2) - dy_G)b_y h\right]^2}{2!} \\ + 2\frac{\partial^2 v_G}{\partial x \partial y}\frac{\left[((i-2) - dx_G)h\right]\left[((l-2) - dy_G)b_y h\right]}{2!} + \ldots,\ p = 3(l-1) \\ + i \text{ with } i, l = 1, 2, 3 \end{aligned} \tag{12}$$

for the 9-point stencils with $dx_G = \frac{x_G - x_5}{h}$ and $dy_G = \frac{y_G - y_5}{b_y h}$,

$$v_p = v_G + \frac{\partial v_G}{\partial x}\left[((i-3)-dx_G)h\right] + \frac{\partial v_G}{\partial y}\left[((l-3)-dy_G)b_y h\right] + \frac{\partial^2 v_G}{\partial x^2}\frac{\left[((i-3)-dx_G)h\right]^2}{2!} + \frac{\partial^2 v_G}{\partial y^2}\frac{\left[((l-3)-dy_G)b_y h\right]^2}{2!} + 2\frac{\partial^2 v_G}{\partial x \partial y}\frac{\left[((i-3)-dx_G)h\right]\left[((l-3)-dy_G)b_y h\right]}{2!} + \ldots,, \; p = 5(l-1)+i \text{ with } i,l = 1,2,3,4,5 \tag{13}$$

for the 25-point stencils with $dx_G = \frac{x_G - x_{13}}{h}$ and $dy_G = \frac{y_G - y_{13}}{b_y h}$ and:

$$w_j = w_G + \frac{\partial w_G}{\partial x}\left[d_{x,j}h\right] + \frac{\partial w_G}{\partial y}\left[d_{y,j}b_y h\right] + \frac{\partial^2 w_G}{\partial x^2}\frac{\left[d_{x,j}h\right]^2}{2!} + \frac{\partial^2 w_G}{\partial y^2}\frac{\left[d_{y,j}b_y h\right]^2}{2!} + 2\frac{\partial^2 w_G}{\partial x \partial y}\frac{\left[(d_{x,j}h)\right]\left[d_{y,j}b_y h\right]}{2!} + \ldots,, \qquad j = 1,2,\ldots,N_G \tag{14}$$

In equations (12) and (13) the function v_p is u_p^*, u_p^{**}, in equation (14) the function w_j is $u_{G,j}^*$, $u_{G,j}^{**}$, $\frac{\partial u_{G,j}^*}{\partial x}$, $\frac{\partial u_{G,j}^{**}}{\partial x}$, $\frac{\partial u_{G,j}^*}{\partial y}$, $\frac{\partial u_{G,j}^{**}}{\partial y}$, N_G is 5 for the 9-point stencils and 11 for the 25-point stencils. The exact solution u_m^* and u_m^{**} to the Poisson equations, equation (1), at the central interface point $x = x_G$ and $y = y_G$ meets the following equations:

$$\frac{\partial^2 u_G^*}{\partial x^2} = -\frac{\partial^2 u_G^*}{\partial y^2} + \frac{1}{e_*}f^*, \qquad \frac{\partial^2 u_G^{**}}{\partial x^2} = -\frac{\partial^2 u_G^{**}}{\partial y^2} + \frac{1}{e_{**}}f^{**}, \tag{15}$$

$$\frac{\partial^{(i+j+2)} u_G^*}{\partial y^i \partial x^{(2+j)}} = -\frac{\partial^{(i+j+2)} u_G^*}{\partial y^{(i+2)} \partial x^j} + \frac{1}{e_*}\frac{\partial^{(i+j)} f^*}{\partial y^i \partial x^j}, \qquad \frac{\partial^{(i+j+2)} u_G^{**}}{\partial y^i \partial x^{(2+j)}} = -\frac{\partial^{(i+j+2)} u_G^{**}}{\partial y^{(i+2)} \partial x^j} + \frac{1}{e_{**}}\frac{\partial^{(i+j)} f^{**}}{\partial y^i \partial x^j} \tag{16}$$

with i, j = 0,1,2,3,4,. . .. equation (16) is obtained by the differentiation of equation (15) with respect to x and y. Inserting equations (12)–(16) with zero source term $f^* = f^{**} = 0$ into equation (11) we will get the following local truncation error in space e:

$$e = b_1 u_G^* + b_2 u_G^{**} + h\left(b_3\frac{\partial u_G^*}{\partial y} + b_4\frac{\partial u_G^{**}}{\partial y} + b_5\frac{\partial u_G^*}{\partial x} + b_6\frac{\partial u_G^{**}}{\partial x}\right) + h^2\left(b_7\frac{\partial^2 u_G^*}{\partial y^2} + b_8\frac{\partial^2 u_G^{**}}{\partial y^2} + b_9\frac{\partial^2 u_G^*}{\partial x \partial y} + b_{10}\frac{\partial^2 u_G^{**}}{\partial x \partial y}\right) + h^3\left(b_{11}\frac{\partial^3 u_G^*}{\partial y^3} + b_{12}\frac{\partial^3 u_G^{**}}{\partial y^3} + b_{13}\frac{\partial^3 u_G^*}{\partial x \partial y^2} + b_{14}\frac{\partial^3 u_G^{**}}{\partial x \partial y^2}\right) + h^4\left(b_{15}\frac{\partial^4 u_G^*}{\partial y^4} + b_{16}\frac{\partial^4 u_G^{**}}{\partial y^4} + b_{17}\frac{\partial^4 u_G^*}{\partial x \partial y^3} + b_{18}\frac{\partial^4 u_G^{**}}{\partial x \partial y^3}\right) + \ldots + h^{11}\left(b_{43}\frac{\partial^{11} u_G^*}{\partial y^{11}} + b_{44}\frac{\partial^{11} u_G^{**}}{\partial y^{11}} + b_{45}\frac{\partial^{11} u_G^*}{\partial x \partial y^{10}} + b_{46}\frac{\partial^{11} u_G^{**}}{\partial x \partial y^{10}}\right) + h^{12}\left(b_{47}\frac{\partial^{12} u_G^*}{\partial y^{12}} + b_{48}\frac{\partial^{12} u_G^{**}}{\partial y^{12}} + b_{49}\frac{\partial^{12} u_G^*}{\partial x \partial y^{11}} + b_{50}\frac{\partial^{12} u_G^{**}}{\partial x \partial y^{11}}\right) + O(h^{13}) \tag{17}$$

where the coefficients b_p (p = 1,2,. . .) are expressed in terms of the coefficients k_i and $q_{1,j}$, $q_{2,j}$ ($i = 1,2,\ldots,M$, $j = 1,2,\ldots,N_G$) and are given in A for the 9-point stencils and in the

attached file 'b-coef-25.nb' for the 25 point stencils. Here we should mention that the expression for the local truncation error, equation (17), includes only the first-order derivatives with respect to x [the higher-order derivatives with respect to x are excluded with the help of equations (15)–(16)].

2.1.1 Homogeneous materials (no interface). For homogeneous materials all a_j (j = 1,2,...,M) coefficients are $a_j = 1$ (see equation (9) if we consider material *), as well as all $q_{1,j} = q_{2,j} = 0$ (j = 1,2,...,N_G) are zero. In this case the derivation of the local truncation error is similar to that in the previous section and is given in our paper (Idesman, 2020) for the 9-point stencils and in our paper (Idesman and Dey, 2020) for the 25-point stencils. These stencils coefficients can be analytically found and for the 9-point stencils they are:

$$k_1 = -\frac{1}{20}\,,\ k_2 = \frac{-5+b_y^2}{10\left(1+b_y^2\right)}\,,\ k_3 = -\frac{1}{20}\,,\ k_4 = \frac{1-5b_y^2}{10\left(1+b_y^2\right)}\,,\ k_5 = 1\,,$$
$$k_6 = \frac{1-5b_y^2}{10\left(1+b_y^2\right)}\,,\ k_7 = -\frac{1}{20}\,,\ k_8 = \frac{-5+b_y^2}{10\left(1+b_y^2\right)}\,,\ k_9 = -\frac{1}{20}\,. \tag{18}$$

with the following local truncation error (see our paper (Idesman, 2020) for details):

$$e = \frac{h^6 b_y^2\left(-1+b_y^2\right)}{400}\frac{\partial^6 u_5^*}{\partial y^6} + \frac{h^8 b_y^2\left(11-32b_y^2+11b_y^4\right)}{100800}\frac{\partial^8 u_5^*}{\partial y^8} + O(h^9)\,, \tag{19}$$

As can be seen from equation (19), for homogeneous materials and square ($b_y = 1$) Cartesian meshes the local truncation error is two orders higher compared to that for rectangular ($b_y \neq 1$) Cartesian meshes.

For homogeneous materials with the 25-point stencils, the stencil coefficients are given in B. They provide the following local truncation error (Idesman and Dey, 2020):

$$e = -\frac{h^{16} y_1}{y_2}\frac{\partial^{16} u_{13}^*}{\partial y^{16}} + O(h^{17})\,, \tag{20}$$

with:

$$y_1 = b_y^4\left(1+b_y^2\right)^2\left(791104 - 6526608b_y^2 + 7168588b_y^4 + 81226757b_y^6 - 288383192b_y^8 + 409496702b_y^{10} - 288383192b_y^{12} + 81226757b_y^{14} + 7168588b_y^{16} - 6526608b_y^{18} + 791104b_y^{20}\right),$$
$$y_2 = (169827840)\left(58288976 - 12041600b_y^2 - 1112834229b_y^4 + 805729100b_y^6 + 7325265506b_y^8 + 805729100b_y^{10} - 1112834229b_y^{12} - 12041600b_y^{14} + 58288976b_y^{16}\right).$$

Remark 4. It was also shown in (Idesman and Dey, 2020) that for homogeneous materials with the 25-point uniform stencils on square ($b_y = 1$) Cartesian meshes, the local truncation

error can be four orders higher compared to that given by equation (20) for rectangular ($b_y \neq 1$) Cartesian meshes.

Remark 5. When the interface cuts just one grid point of the 9-point or 25-point stencils, we can still use cut stencils for homogeneous materials. In this case, we have 8-point or 24-point cut stencils for homogeneous materials.

The stencils coefficients of the cut stencils can be derived by zeroing $k_i = 0$ (i is the number of the grid point cut by the interface). Then, the stencil coefficients and the corresponding local truncation errors of the cut stencils can be analytically found similar to the procedure for the non-cut stencils (Idesman, 2020; Idesman and Dey, 2020). The orders of the local truncation error of the cut stencils are 4 for the 8-point cut stencils and 14 for the 24-point cut stencils (these orders are the same or higher compared to those considered below for the stencils with interfaces).

2.1.2 Heterogeneous materials with an irregular interface. For the interface represented by an inclined line, some analytical results for the 9-point and 25-point stencils that include the grid points with different material properties can be obtained with the help of Mathematica. We have found that the maximum order of the local truncation error is 4 for the 9-point stencils and 12 for the 25-point stencils. The minimum number of interface points needed for this accuracy is $N_G = 3$ for the 9-point stencils and $N_G = 11$ for the 25-point stencils. However, numerical results show that for the 9-point stencils the absolute accuracy (at the same order of accuracy) can be increased by the use of $N_G = 5$. Therefore, for our approach, we will use $N_G = 5$ for the 9-point stencils and $N_G = 11$ for the 25-point stencils.

To obtain the same order of accuracy for the general shape of the interface we will use the following procedure for the 9-point and 25-point stencils.*a) 9-point stencils with an irregular interface*

We use the 18 unknown stencil coefficients k_i (i = 1, 2, 3, 4, 6, 7, 8, 9 with $k_5 = 1$) and $q_{1,j}$, $q_{2,j}$ (j = 1,2,. . .,5) to minimize the local truncation error, equation (17). First, we zero the first 14 coefficients b_p in equation (17) up to the third order with respect to h; i.e.

$$b_p = 0\,, \qquad p = 1, 2, \ldots, 14\,. \tag{21}$$

Then, to have a sufficient number of equations for the calculation of the 18 unknown stencil coefficients k_i (i = 1, 2, 3, 4, 6, 7, 8, 9) and $q_{1,j}$, $q_{2,j}$ (j = 1, 2,. . ., 5), we use the least square method for the minimization of coefficients b_p related to the fourth, fifth and sixth orders of the local truncation error with the following residual R:

$$R = \sum_{p=15}^{18} b_p^2 + h_1 \sum_{p=19}^{22} b_p^2 + h_2 \sum_{p=23}^{26} b_p^2\,, \tag{22}$$

where h_1 and h_2 are the weighting factors to be selected (e.g. the numerical experiments show that $h_1 = h_2 = 0.1$ yields accurate results). To minimize the residual R with the constraints given by equation (21), we can form a new residual $\overline{R}$ with the Lagrange multipliers λ_l:

$$\overline{R} = \sum_{l=1}^{14} \lambda_l b_l + \sum_{p=15}^{18} b_p^2 + h_1 \sum_{p=19}^{22} b_p^2 + h_2 \sum_{p=23}^{26} b_p^2\,. \tag{23}$$

The residual $\overline{R}$ is a quadratic function of the stencil coefficients k_i (i = 1, 2,. . ., 9) and $q_{1,j}$, $q_{2,j}$ (j = 1, 2,. . ., 5) and a linear function of the Lagrange multipliers λ_l; i.e.

$\overline{R} = \overline{R}(k_i, q_{1,j}, q_{2,j}, \lambda_l)$. In order minimize the residual $\overline{R} = \overline{R}(k_i, q_{1,j}, q_{2,j}, \lambda_l)$, the following equations based on the least square method for the residual $\overline{R}$ can be written down:

$$\frac{\partial \overline{R}}{\partial k_i} = 0\,, \qquad \frac{\partial \overline{R}}{\partial q_{1,j}} = 0\,, \qquad \frac{\partial \overline{R}}{\partial q_{2,j}} = 0\,, \qquad \frac{\partial \overline{R}}{\partial \lambda_l} = 0\,, \qquad (24)$$
$$i = 1, 2, \ldots, 9\,, \qquad j = 1, 2, \ldots, 5\,, \qquad l = 1, 2, \ldots, 14\,,$$

where equation $\frac{\partial \overline{R}}{\partial k_5} = 0$ in equation (24) should be replaced by $k_5 = 1$; Remark 3 [equation (24)] forms a system of 33 linear algebraic equations with respect to 33 coefficients k_i ($i = 1, 2, \ldots, 9$) and $q_{1,j}$, $q_{2,j}$ ($j = 1, 2, \ldots, 5$), as well as 14 Lagrange multipliers λ_l ($l = 1, 2, \ldots, 14$). Solving these linear algebraic equations numerically, we can find the coefficients k_i ($i = 1, 2, \ldots, 9$) for the 9-point uniform stencils, as well as $q_{1,j}$, $q_{2,j}$ ($j = 1, 2, \ldots, 5$). As can be seen from equation (17), the presented procedure provides the fourth order of the local truncation error for the 9-point uniform stencils with the general geometry of the interface. The 9-point uniform stencils of OLTEM for a homogeneous material (without interface) provide the sixth order of the local truncation error for rectangular meshes [equation (19)]. In this case, the global error is defined by the order of accuracy of the 9-point stencils with interfaces. This leads to the third order of accuracy of global solutions; see the numerical examples below. Moreover, due to the minimization of the leading high-order terms b_p of the local truncation error in equation (23), at the same numbers of degrees of freedom the new approach on irregular interfaces yields more accurate results than those obtained by high-order finite elements (up to the fourth-order) with much wider stencils; see the numerical examples below.

The global discrete system of equations includes the 9-point stencils for homogeneous materials without interfaces and the 9-point stencils for heterogeneous materials with interfaces between different materials (Figure 1) for all internal grid points located inside the domain. The new approach does not use unknowns at the interfaces and the global discrete system of equations has the same unknowns for homogeneous and heterogeneous materials (the same structures of the sparse global matrices, the difference is only in the values of the stencil coefficients k_p of the global matrices for homogeneous and heterogeneous materials).

b) 25-point stencils with an irregular interface

We use the 46 unknown stencil coefficients k_i ($i = 1, 2, \ldots, 12, 14, 15, \ldots, 25$ with $k_{13} = 1$) and $q_{1,j}$, $q_{2,j}$ ($j = 1, 2, \ldots, 11$) to minimize the local truncation error [equation (17)]. The analysis of the local truncation error for the inclined interface shows that some coefficients b_p starting with $i > 30$ are linearly dependent. Therefore, we will use the following procedure. First, we will zero the first 30 coefficients b_p in equation (17) up to the 7-th order with respect to h; i.e.

$$b_p = 0\,, \qquad p = 1, 2, \ldots, 30\,. \qquad (25)$$

Then, to have a sufficient number of equations for the calculation of the 46 stencil coefficients k_i ($i = 1, 2, \ldots, 12, 14, 15, \ldots, 25$) and $q_{1,j}$, $q_{2,j}$ ($j = 1, 2, \ldots, 11$), we use the least square method for the minimization of coefficients b_p related to the 8-th and higher orders of the local truncation error with the following residual R:

$$R = \sum_{p=31}^{34} b_p^2 + h_1 \sum_{p=31}^{38} b_p^2 + h_2 \sum_{p=39}^{42} b_p^2 + h_3 \sum_{p=43}^{46} b_p^2 + h_4 \sum_{p=47}^{50} b_p^2\,, \qquad (26)$$

where h_1, h_2, h_3, h_4 are the weighting factors to be selected. Using larger values of h_i (i = 1, 2, 3, 4) for the lower order terms in equation (26) we can practically zero the coefficients b_p for the lower order terms in equation (26) [e.g. the numerical experiments show that $h_1 = 0.1$, $h_2 = 0.01$, $h_3 = 0.001$, $h_4 = 0.0001$ can practically zero b_p (p = 31, 32,. . ., 46) up to the 11-th order in equation (17)]. To minimize the residual R with the constraints given by equation (25), we can form a new residual $\overline{R}$ with the Lagrange multipliers λ_l:

$$\overline{R} = \sum_{l=1}^{30} \lambda_l b_l + \sum_{p=31}^{34} b_p^2 + h_1 \sum_{p=31}^{38} b_p^2 + h_2 \sum_{p=39}^{42} b_p^2 + h_3 \sum_{p=43}^{46} b_p^2 + h_4 \sum_{p=47}^{50} b_p^2 . \tag{27}$$

The residual $\overline{R}$ is a quadratic function of the stencil coefficients k_i (i = 1, 2,. . ., 25) and $q_{1,j}$, $q_{2,j}$ (j = 1, 2,. . ., 11) and a linear function of the Lagrange multipliers λ_l; i.e. $\overline{R} = \overline{R}(k_i, q_{1,j}, q_{2,j}, \lambda_l)$. In order minimize the residual $\overline{R} = \overline{R}(k_i, q_{1,j}, q_{2,j}, \lambda_l)$, the following equations based on the least square method for the residual $\overline{R}$ can be written down:

$$\begin{aligned} &\frac{\partial \overline{R}}{\partial k_i} = 0 , \qquad \frac{\partial \overline{R}}{\partial q_{1,j}} = 0 , \qquad \frac{\partial \overline{R}}{\partial q_{2,j}} = 0 , \qquad \frac{\partial \overline{R}}{\partial \lambda_l} = 0 , \\ &i = 1, 2, \ldots, 25 , \qquad j = 1, 2, \ldots, 11 , \qquad l = 1, 2, \ldots, 30 , \end{aligned} \tag{28}$$

where equation $\frac{\partial \overline{R}}{\partial k_{13}} = 0$ in equation (28) should be replaced by k_{13} = 1; Remark 3 [equation (28)] forms a system of 77 linear algebraic equations with respect to 47 unknown coefficients k_i (i = 1, 2,. . ., 25) and $q_{1,j}$, $q_{2,j}$ (j = 1, 2,. . ., 11), as well as 30 Lagrange multipliers λ_l (l = 1, 2,. . ., 30). Solving these linear algebraic equations numerically, we can find the coefficients k_i (i = 1, 2,. . ., 25) for the 25-point uniform stencils, as well as $q_{1,j}$, $q_{2,j}$ (j = 1, 2,. . ., 11). The presented procedure provides the 12-th order of the local truncation error for the 25-point uniform stencils with the general geometry of the interface. The 25-point uniform stencils of OLTEM for a homogeneous material (without interface) provide the 16-th order of the local truncation error for rectangular meshes [equation (19)]. In this case the global error is defined by the order of accuracy of the 25-point stencils with interfaces. This leads to the 11-th order of accuracy of global solutions; see the numerical examples below. Moreover, due to the minimization of the leading high-order terms b_p of the local truncation error in equation (27), at the same numbers of degrees of freedom the new approach with irregular interfaces yields more accurate results than those obtained by high-order finite elements (up to the 7-th order) with much wider stencils; see the numerical examples below. Unfortunately, we could not compare our results using finite elements with the 8-th and higher orders because the 7-th order is the highest order of finite elements in the commercial software 'COMSOL.'

Remark 6. To estimate the computational costs of the solution of 33 (for the 9-point stencils) and 77 (for the 25-point stencils) linear algebraic equations formed by equation (24) for the 9-point stencils and by equation (28) for the 25-point stencils, we solved 10^6 such systems of algebraic equations with the general MATLAB solver 'pinv' on a simple student laptop computer (Processor: Intel (R) Core(TM) i5-4210U CPU @ 1.70GHz 2.40GHz). The computation 'wall' time was T = 7,452.08 s and T = 45,774.63 s for 10^6 systems or the average time for one system was 0.007452 s for the 9-point stencils and 0.045774 s for the 25-point stencils. Because the coefficients k_i are independently calculated for different stencils,

the computation time of their calculation for different stencils can be significantly reduced on modern parallel computers. This means that for large global systems of equations, the computation time for the calculation of the coefficients k_i is very small compared to that for the solution of the global system of algebraic equations. We should mention that the coefficients $q_{1,j}$, $q_{2,j}$ calculated from the local system of equations, equations (24) and (28), are only used for the calculation of non-zero right-hand side vector while the Lagrange multipliers λ_l in the local system of equations, equations (24) and (28), are not used in the global system of equations at all.

Remark 7. It is interesting to mention that the stencil coefficients can be also derived using the central grid point with the coordinates x_5 and y_5 for the 9-point stencil or x_{13} and y_{13} for the 25-point stencil in equations (12)–(17) instead of the interface point with the coordinates x_G and y_G.

The global discrete system of equations includes the 25-point stencils for homogeneous materials without interfaces and the 25-point stencils for heterogeneous materials with interfaces between different materials (Figure 2) for all internal grid points located inside the domain. The new approach does not use unknowns at the interfaces and the global discrete system of equations has the same unknowns for homogeneous and heterogeneous materials (the same structures of the sparse global matrices, the difference is only in the values of the stencil coefficients k_p [equation (9)] of the global matrices for homogeneous and heterogeneous materials).

2.2 Nonzero source term $f_l \neq 0$ in equation (1)

The inclusion of non-zero source term f_l in the partial differential equations, equation (1), leads to the non-zero term $\overline{f}$ in the stencil equation, equation (9) [similar to equation (3)]. As we mentioned after equation (2), the functions f_l can be discontinuous across the interfaces. The expression for the term $\overline{f}$ can be calculated from the procedure used for the derivation of the local truncation error in the case of zero source term as follows. Below we show the derivations for the 9-point stencils (the derivations for the 25-point stencils are similar). In the case of non-zero source term $f_l(\mathbf{x}) \neq 0$ and $\overline{f} \neq 0$, the insertion of equations (12)–(16) into equation (11) yields the following local truncation error in space e_f:

$$
\begin{aligned}
e_f = e - [\overline{f} - \frac{1}{2}\mathbf{h}^2((q_{1,2}d_{x,2}^2 + a_1(dx_G+1)^2k_1 + a_3k_3 + a_4k_4 + a_6k_6 + a_7k_7 + a_9k_9 \\
+ dx_G(dx_G(a_2k_2 + a_3k_3 + a_4k_4 + a_5k_5 + a_6k_6 + a_7k_7 + a_8k_8 + a_9k_9) \\
- 2(a_3k_3 - a_4k_4 + a_6k_6 - a_7k_7 + a_9k_9)) + 2d_{x,5}e_*n_{x,5}q_{2,5} + d_{x,3}^2q_{1,3} + d_{x,4}^2q_{1,4} \\
+ d_{x,5}^2q_{1,5} + 2e_*(d_{x,2}n_{x,2}q_{2,2} + d_{x,3}n_{x,3}q_{2,3} + d_{x,4}n_{x,4}q_{2,4}))(\tilde{f}_G^*) \\
+ (-q_{1,2}d_{x,2}^2 - (a_1-1)(dx_G+1)^2k_1 - a_3k_3 + k_3 - a_4k_4 + k_4 - a_6k_6 + k_6 - a_7k_7 \\
+ k_7 - a_9k_9 + k_9 + dx_G(2((a_3-1)k_3 - a_4k_4 + k_4 + (a_6-1)k_6 - a_7k_7 + k_7 + (a_9-1)k_9) \\
+ dx_G(-a_2k_2 + k_2 - a_3k_3 + k_3 - a_4k_4 + k_4 - a_5k_5 + k_5 - a_6k_6 + k_6 - a_7k_7 + k_7 \\
- a_8k_8 + k_8 - a_9k_9 + k_9)) - 2d_{x,5}e_{**}n_{x,5}q_{2,5} - d_{x,3}^2q_{1,3} - d_{x,4}^2q_{1,4} - d_{x,5}^2q_{1,5} \\
- 2e_{**}(d_{x,2}n_{x,2}q_{2,2} + d_{x,3}n_{x,3}q_{2,3} + d_{x,4}n_{x,4}q_{2,4}))(\tilde{f}_G^{**})) - \mathbf{h}^3 \ldots],
\end{aligned}
\tag{29}
$$

where e is the local truncation error in space given by equation (17) for zero source term, $\tilde{f}_G^*$ and $\tilde{f}_G^{**}$ designate functions $\frac{f^*(x,y)}{e_*}$ and $\frac{f^{**}(x,y)}{e_{**}}$ calculated at the interface point with the coordinates $x = x_G$ and $y = y_G$. Equating to zero the expression in the square brackets in the right-hand side of equation (29), we will get the expression for $\bar{f}$:

$$\begin{aligned}\bar{f} = \frac{1}{2}\mathbf{h}^2((&q_{1,2}d_{x,2}^2 + a_1(dx_G+1)^2k_1 + a_3k_3 + a_4k_4 + a_6k_6 + a_7k_7 + a_9k_9\\ &+ dx_G(dx_G(a_2k_2 + a_3k_3 + a_4k_4 + a_5k_5 + a_6k_6 + a_7k_7 + a_8k_8 + a_9k_9)\\ &- 2(a_3k_3 - a_4k_4 + a_6k_6 - a_7k_7 + a_9k_9)) + 2d_{x,5}e_*n_{x,5}q_{2,5} + d_{x,3}^2q_{1,3} + d_{x,4}^2q_{1,4}\\ &+ d_{x,5}^2q_{1,5} + 2e_*(d_{x,2}n_{x,2}q_{2,2} + d_{x,3}n_{x,3}q_{2,3} + d_{x,4}n_{x,4}q_{2,4}))(\tilde{f}_G^*)\\ &+ (-q_{1,2}d_{x,2}^2 - (a_1-1)(^{dx_G+1)2}k_1 - a_3k_3 + k_3 - a_4k_4 + k_4 - a_6k_6 + k_6 - a_7k_7 + k_7\\ &- a_9k_9 + k_9\\ &+ dx_G(2((a_3-1)k_3 - a_4k_4 + k_4 + (a_6-1)k_6 - a_7k_7 + k_7 + (a_9-1)k_9)\\ &+ dx_G(-a_2k_2 + k_2 - a_3k_3 + k_3 - a_4k_4 + k_4 - a_5k_5 + k_5 - a_6k_6 + k_6 - a_7k_7 + k_7\\ &- a_8k_8 + k_8 - a_9k_9 + k_9)) - 2d_{x,5}e_{**}n_{x,5}q_{2,5} - d_{x,3}^2q_{1,3} - d_{x,4}^2q_{1,4} - d_{x,5}^2q_{1,5}\\ &- 2e_{**}(d_{x,2}n_{x,2}q_{2,2} + d_{x,3}n_{x,3}q_{2,3} + d_{x,4}n_{x,4}q_{2,4}))(\tilde{f}_G^{**})) + \mathbf{h}^3...,\end{aligned} \tag{30}$$

as well as we will get the same local truncation errors $e_f = e$ for zero and non-zero source term (see C for the detailed expression of $\bar{f}$). This means that the coefficients k_i ($i = 1, 2,\ldots$, M) of the stencil equations are first calculated for zero source term $f_l = 0$ as described in Section 2.1. Then, the nonzero source term $\bar{f}$ given by equation (30) is used in the stencil equation [equation (9)]. The explicit expression for $\bar{f}$ for the 25-point stencils is given in the attached file 'RHS-25.nb.'

3. Numerical examples

In this section, the computational efficiency of the OLTEM with the 9-point and 25-point stencils developed for the solution of the Poisson equation with discontinuous coefficients will be demonstrated and compared with conventional linear and high order (up to 7-th order, the highest order in 'COMSOL') triangular and quadrilateral finite elements. In the numerical results presented below 'T' and 'Q' refer to the triangular and quadrilateral finite elements. For OLTEM with the 25 points stencils, the high-order numerical boundary conditions similar to those developed in (Idesman, 2018) are used. For finite element calculations, the commercial finite element software 'COMSOL' with isoparametric finite elements is used. Similar to the finite element terminology, a grid point of a Cartesian mesh used for OLTEM will be called a node. To compare the accuracy of OLTEM with FEM, the following errors are considered in the sections below. The relative errors e_u^j for the function u at the j-th node is defined as:

$$e_u^j = \frac{|u_j^{num} - u_j^{exact}|}{u_{max}^{exact}}, \qquad j = 1, 2, \ldots, N. \tag{31}$$

The maximum relative errors e_u^{max} for the function u is defined as:

$$e_u^{max} = \max_j e_u^j, \qquad j = 1, 2, \ldots, N. \tag{32}$$

In equations (31)–(32) the superscripts 'num' and 'exact' correspond to the numerical and exact solutions, N is the total number of the grid points used in calculations, u_{max}^{exact} is the maximum absolute value of the exact (reference) solution for the function over the entire domain. The use of u_{max}^{exact} instead of u_j^{exact} in the denominator of equation (31) allows us to apply equation (31) even if the exact solution at grid point j is zero [equation (34)]. We also use the L^2 error norm for finite elements (Bathe, 1996) and the l^2 error norm (Langtangen and Linge, 2017) for OLTEM:

$$e_u^{l^2} = \left\{ dx\, dy \sum_{i=0}^{N_x} \sum_{j=0}^{N_y} \left[u^{num}(x_i, y_j) - u^{exact}(x_i, y_j) \right]^2 \right\}^{\frac{1}{2}} / |u^{exact}|_{L^2}, \tag{33}$$

where N_x and N_y are the numbers of Cartesian grid points along x- and y-axes, x_i and y_j are the coordinates of Cartesian grid points.

3.1 Two-dimensional bi-material plate with inclined interface

Let us consider the two-dimensional Poisson equation with discontinuous coefficients for the bi-material plate *ABCDEF* shown in Figure 3(a). The plate consists of two trapezoidal plates *ABCF* (subdomain Ω_I) and *CDEF* (subdomain Ω_{II}) connected through an inclined interface *EF* with $\theta = 35^\circ$. The following material properties are used for the Poisson equation in two subdomains: $e_I = 1/g_1$ in Ω_I and $e_{II} = 1$ in Ω_{II} where we vary the constant g_1 to consider different contrasts $\frac{e_{II}}{e_I} = g_1$.

We use the following exact solution to the Poisson equation for this problem:

$$u(x,y) = \begin{cases} cos\{15(xcos\theta + ysin\theta)\} sin\{g_1(-xsin\theta + ycos\theta)\} & \text{in} \quad \Omega_I \\ cos\{15(xcos\theta + ysin\theta)\} sin(-xsin\theta + ycos\theta) & \text{in} \quad \Omega_{II} \end{cases} \tag{34}$$

and non-zero source $f_I(x,y) = -\frac{1}{g_1}\left(g_1^2 + 225\right) cos\{15(xcos\theta + ysin\theta)\} sin\{g_1(-xsin\theta + ycos\theta)\}$ in Ω_I and $f_{II}(x,y) = -226 cos\{15(xcos\theta + ysin\theta)\} sin(-xsin\theta + ycos\theta)$ in Ω_{II} calculated according to equation (1).

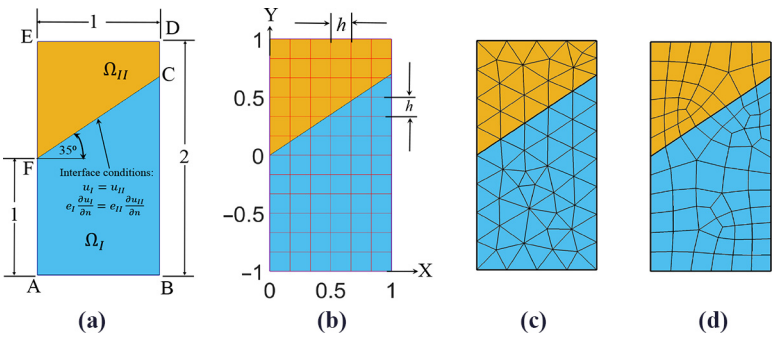

Figure 3.
A two-dimensional bi-material plate *ABCDEF* with an inclined interface *FC* (a). Examples of a Cartesian mesh for OLTEM (b) as well as meshes with triangular (c) and quadrilateral (d) finite elements generated by the commercial software COMSOL

The Dirichlet boundary conditions along AB, BD, DE and EA are imposed according to the exact solution, equation (34). The problem is solved by OLTEM with the 9-point and 25-point stencils for different contrasts $\frac{e_{II}}{e_I}$. Figure 3(b) shows a typical square (b_y = 1) Cartesian mesh used for OLTEM. Figure 4 shows the distribution of the exact solution for the function u with the contrast $\frac{e_{II}}{e_I} = 10$, as well as the distribution of the relative error in the numerical solutions for the function u obtained by OLTEM with the 9-point and 25-point stencils on a square (b_y = 1) Cartesian mesh of size h = 1/18. As can be seen from Figure 4(b) and 4(c), the results obtained by OLTEM are accurate (the errors are small). It can be also seen that the maximum error occurs close to the interface. This can be explained by the difference of accuracy of the stencils used for the grid points located far from the interface and the stencils affected by the interface (Sections 2.1.1 and 2.1.2).

Figure 5 shows the maximum error e_u^{max} as a function of the mesh size h in the logarithmic scale for OLTEM with the 9-point [Figure 5(a)] and 25-point [Figure 5(b)] stencils with different contrasts. As can be seen from Figure 5(a), the order of convergence of OLTEM with the 9-point stencils is greater than three for all considered contrasts. Figure 5(b) shows that the order of convergence of OLTEM with the 25-point stencils is greater than 11 for different contrasts. This means OLTEM retains the order of convergence regardless of the contrast. These observations are in agreement with the theoretical results in Section 2.

To study the convergence and stability of the numerical results obtained by OLTEM in more detail, Figure 6 presents the curves in Figure 5 at small changes of the Cartesian mesh size h_i [Curves 1, 2, 3, 4 in Figure 5(a) and 5(b) correspond to Curves 1, 2, 3, 4 in Figures 6(a) and 6(b)]. For this study, we solve the test problem on 1001 Cartesian meshes using the following equation for the mesh size h_i (i = 1, 2,. . ., 1001):

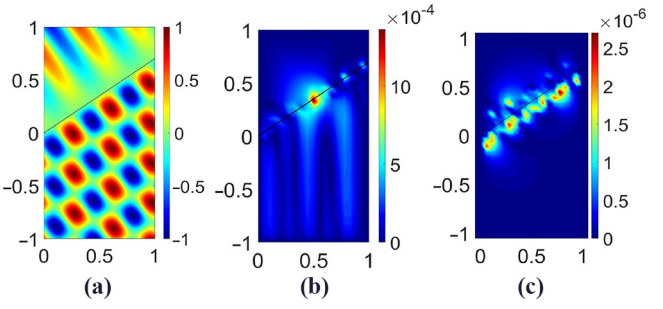

Figure 4.
The distribution of the exact solution for the function u (a) [equation (34)] and the relative errors e_u (b, c) for the two-dimensional plate with the inclined interface [Figure 3(a)]. The numerical solutions of the two-dimensional Poisson equation with the contrast $\frac{e_{II}}{e_I} = 10$ are obtained by OLTEM with the 9-point (b) and 25-point (c) stencils on the square (b_y = 1) Cartesian mesh of size h = 1/18

$$h_i = h_1 + \frac{(h_2 - h_1)}{1000}(i-1)\,, \qquad i = 1, 2, \ldots, 1001 \tag{35}$$

where h_1 and h_2 are the maximum and minimum mesh sizes that can be found from Figure 6 for different curves. As can be seen from Figure 6, the errors for OLTEM with the 9-point and 25-point stencils smoothly decrease with the decrease in the mesh size h for the different contrasts considered in the analysis. This means OLTEM yields stable and convergent numerical results.

Next, for the contrast $\frac{e_{II}}{e_I} = 10$ we compare the results obtained by OLTEM with the 9-point and 25-point stencils with those obtained by linear and high-order finite elements. Figure 3(c) and 3(d) shows examples of meshes with triangular and quadrilateral finite elements generated by COMSOL. Figure 7 presents the error e_u^{max} as a function of the number N of degrees of freedom in the logarithmic scale at mesh refinement. As can be seen from Figure 7, at the same N the numerical results obtained by OLTEM with the 25-point stencils are much more accurate than those obtained by linear and high-order (up to the 7-th order) finite elements. It can be also seen from Figure 7 that OLTEM with the 9-point stencils yields more accurate results than those by obtained finite elements up to the 4-th order. Furthermore, up to the engineering accuracy of 0.1% (–3 in the logarithmic scale

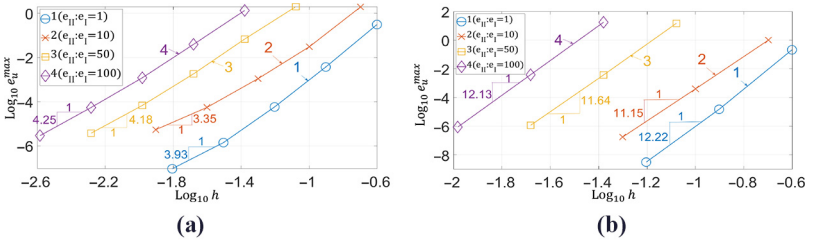

Figure 5. The maximum relative errors e_u^{max} as a function of the mesh size h at mesh refinement in the logarithmic scale for the two-dimensional plate with the inclined interface [Figure 3(a)]

Notes: The numerical solutions of the two dimensional Poisson equation are obtained by OLTEM with the 9-point (a) and 25- point (b) stencils on uniform square ($b_y = 1$) Cartesian meshes with the following contrasts: $\frac{e_{II}}{e_I} = 1$(curve 1), $\frac{e_{II}}{e_I} = 10$ (curve 2), $\frac{e_{II}}{e_I} = 50$ (curve 3) and $\frac{e_{II}}{e_I} = 100$ (curve 4)

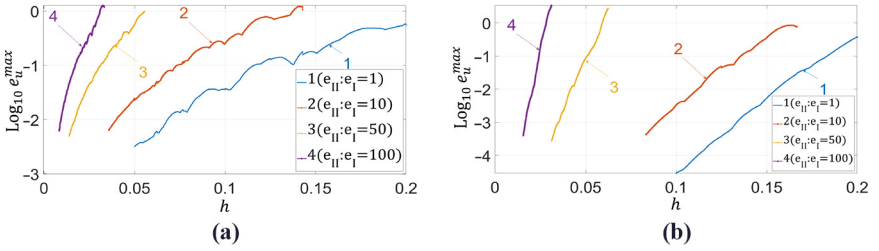

Figure 6. The logarithm of the maximum relative errors e_u^{max} as a function of the mesh size h for the two-dimensional plate with the inclined interface [Figure 3(a)]

Notes: The numerical solutions of the twodimensional Poisson equation are obtained by OLTEMwith the 9-point (a) and 25- point (b) stencils on uniform square ($b_y = 1$) Cartesian meshes with the following contrasts: $\frac{e_{II}}{e_I} = 1$ (curve 1), $\frac{e_{II}}{e_I} = 10$ (curve 2), $\frac{e_{II}}{e_I} = 50$ (curve 3) and $\frac{e_{II}}{e_I} = 100$ (curve 4). Each curve is calculated on 1001 meshes

along the y-axis in Figure 7) the results obtained by OLTEM with the 9-point stencils are more accurate than those obtained by finite elements up to the 7-th order. This huge increase in accuracy by OLTEM compared to that for high-order finite elements is impressive because high-order finite elements have much wider stencils and require a much greater computation time. For example, the 7-th order (septic) quadrilateral finite element have 225-point stencils on uniform meshes compared to OLTEM with the 9-point and 25-point stencils used in the paper. A similar convergence for OLTEM and its comparison with finite elements in the L^2 error norm are obtained in Figure 8. As can be seen, the numerical results obtained by OLTEM with the 25-point stencils are much more accurate than those obtained by linear and high-order (up to the 7-th order) finite elements.

It is interesting to mention that at the same N triangular finite elements yield more accurate results compared to those for quadrilateral finite elements; see curves 3–9 in Figure 7(a) and 7(b). Therefore, we use triangular finite elements for the problem considered in the next section.

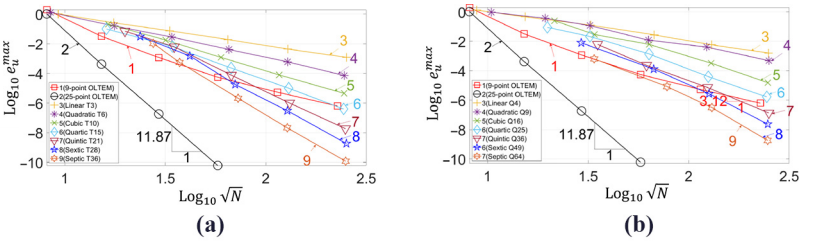

Figure 7.
The maximum relative error e_u^{max} as a function of $\sqrt{N}$ in the logarithmic scale at mesh refinement for the two-dimensional plate with the inclined interface [Figure 3(a)]; N is the number of degrees of freedom

Notes: The numerical solutions of the twodimensional Poisson equation with the contrast $\frac{e_{II}}{e_I} = 10$ are obtained by OLTEM with the 9-point (curve 1) and 25-point (curve 2) stencils on uniform square ($b_y = 1$) Cartesian meshes, as well as by linear and high-order triangular (a) and quadrilateral (b) finite elements (curves 3 – 9). Curves 3, 4,. . .,9 correspond to linear, quadratic,. . ., the 7-th order elements

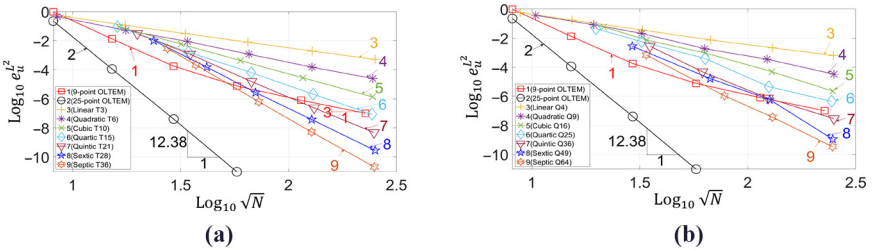

Figure 8.
The L^2 error norm $e_u^{L^2}$ as a function of $\sqrt{N}$ in the logarithmic scale at mesh refinement for the two-dimensional plate with the inclined interface [Figure 3(a)]; N is the number of degrees of freedom

Notes: The numerical solutions of the twodimensional Poisson equation with the contrast $\frac{e_{II}}{e_I}$ =10 are obtained by OLTEM with the 9-point (Curve 1) and 25-point (Curve 2) stencils on uniform square ($b_y = 1$) Cartesian meshes, as well as by linear and high-order triangular (a) and quadrilateral (b) finite elements (Curves 3 – 9). Curves 3, 4,. . .,9 correspond to linear,quadratic,. . ., the 7-th order elements

3.2 Two-dimensional bi-material plate with circular interface

Let us consider the two-dimensional Poisson equation with discontinuous coefficients for a bi-material plate *ABCD* shown in Figure 9(a). The plate consists of an outer subdomain (subdomain Ω_I) and a circular inner subdomain centered at $O(0.5, 0.5)$ with radius $r = 0.25$ (subdomain Ω_{II}) connected through the circular interface. The coefficient e is $e_I = 5$ for the outer subdomain Ω_I and $e_{II} = 1$ for the circular subdomain Ω_{II} with the contrast $\frac{e_{II}}{e_I} = 1/5$. The source term in the Poisson equation is chosen to be $f_I(x,y) = 0$ for Ω_I and $f_{II}(x,y) = 5000cos(15\pi x + 9\pi y)$ for Ω_{II}. The following Dirichlet boundary conditions are applied: $u(y) = 1 + 2sin\left(\frac{11\pi y}{2}\right)$ along the edge AD, $u(y) = ycos(2\pi y)$ along the edge BC, $u(x) = 2x^4 - 2x^3 + x^2 - 2x + 1$ along the edge AB and $u(x) = -cos(5\pi x)$ along the edge AB. The exact solution for this problem is unknown. Therefore, the numerical solution obtained by the 7-th order triangular finite element on a mesh of 2, 626, 555 degrees of freedom is used as the reference solution for the calculation of the errors. Figure 10(a) shows the distribution of the function u for the reference solution.

This problem is solved by linear and high order triangular finite elements, as well as by OLTEM with the 9-point and 25-point stencils. Figure 9(b) and 9(c) shows examples of a Cartesian mesh used for OLTEM and a mesh with triangular linear finite elements generated by COMSOL.

To estimate the order of convergence of OLTEM and to compare the accuracy of the numerical solutions obtained by different techniques we select the point $O(0.5, 0.5)$ and plot the error e_u^O at this point O; see Figure 10(b) with the errors plotted in the logarithmic scale at mesh refinement. It can be seen from Figure 10(b) that at the same number N of degrees of freedom, OLTEM with the 25-point stencils yields much more accurate results than those obtained by linear and high-order finite elements (similar results can be obtained at other points). On the other hand OLTEM with the 9-point stencils yields more accurate results than those obtained by finite elements up to the 4-th order.

Furthermore, up to the engineering accuracy of 1% (–2 in the logarithmic scale along the y-axis in Figure 10(b) the results obtained by OLTEM with the 9-point stencils are more accurate than those obtained by finite elements up to the 7-th order. It can also be seen from Figure 10(b) that OLTEM with the 9-point and 25-point stencils shows close to the 3-rd and

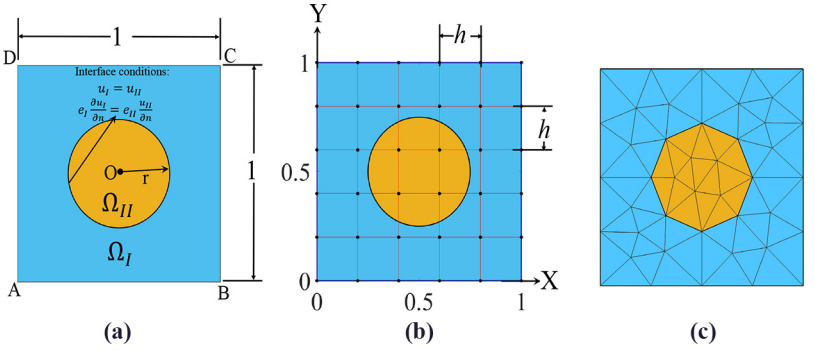

Figure 9.
A two-dimensional bi-material plate *ABCD* with a circular interface centered at $O(0.5, 0.5)$ with a radius $r = 0.25$(a). Examples of a Cartesian mesh for OLTEM (b) as well as a mesh with linear triangular finite elements (c) generated by the commercial software COMSOL

11-th order of accuracy at mesh refinement (the mesh size is approximately proportional to $\sqrt{N}$).

3.3 Two-dimensional bi-material plate with elliptical interface

Let us consider the two-dimensional Poisson equation with discontinuous coefficients for a bi-material plate *ABCD* shown in Figure 11(a). The plate consists of an outer subdomain (subdomain Ω_I) and an elliptical inner subdomain (subdomain Ω_{II}) centered at (0, 0) with the interface described by the following equation:

$$\frac{x^2}{\alpha^2}+\frac{y^2}{\beta^2}=1\,, \tag{36}$$

where $\alpha = 0.25$ and $\beta = 0.08$. The coefficient e is $e_I = 1$ for the outer subdomain Ω_I and $e_{II} = 50$ for the elliptical subdomain Ω_{II} with the contrast $\frac{e_{II}}{e_I} = 50$.

Using the method of manufactured solution, the following exact solution to the Poisson equation is selected:

$$u(x,y)=\begin{cases} cos\left(\dfrac{x^2}{\alpha^2}+\dfrac{y^2}{\beta^2}\right) & \text{in} \quad \Omega_I \\ \dfrac{1}{50}\left[cos\left(\dfrac{x^2}{\alpha^2}+\dfrac{y^2}{\beta^2}\right)+49cos(1)\right] & \text{in} \quad \Omega_{II} \end{cases} \tag{37}$$

This solution meets the interface conditions, equation (2). The source term in the Poisson equation and the Dirichlet boundary conditions along *AB*, *BC*, *CD* and *DA* are calculated according to the exact solution equation (37). This problem is solved by linear and high order triangular finite elements, as well as by OLTEM with the 9-point and 25-point stencils.

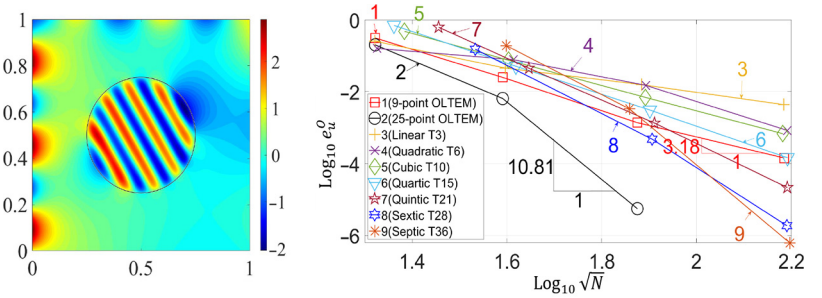

Figure 10.
a) Distribution of the reference solution for the function u for the plate with the circular interface. The reference solution is obtained by the 7-th order triangular finite elements with 2,626,555 degrees of freedom; b) The maximum relative error e_u^O at point O (0.5, 0.5) as a function of $\sqrt{N}$ in the logarithmic scale at mesh refinement for the two-dimensional plate with the circular interface; N is the number of degrees of freedom

Notes: The numerical solutions of the twodimensional Poisson equation are obtained by OLTEMwith the 9-point (Curve 1) and 25-point (Curve 2) stencils on uniform square ($b_y = 1$) Cartesian meshes, as well as by linear and high-order triangular finite elements (Curves 3 – 9). Curves 3, 4,. . .,9 correspond to linear, quadratic,. . ., the 7-th order elements

Figure 11(b) and 11(c) shows examples of a Cartesian mesh used for OLTEM and a mesh with linear triangular finite elements generated by COMSOL.

To estimate the order of convergence of OLTEM and to compare the accuracy of the numerical solutions obtained by different techniques, Figure 12 shows the maximum relative error e_u^{max} and the L^2 error norm $e_u^{L^2}$ as a function of number of degrees of freedom in the logarithmic scale. As can be seen from Figure 12, at the same N the numerical results obtained by OLTEM with the 25-point stencils are much more accurate than those obtained by linear and high-order (up to the 7-th order) finite elements. It can be also seen from Figure 12 that OLTEM with the 9-point stencils yields more accurate results than those by obtained finite elements up to the 4-th order. Furthermore, up to the engineering accuracy of 1% (–2 in the logarithmic scale along the y-axis in Figure 12) the results obtained by OLTEM with the 9-point stencils are more accurate than those obtained by finite elements up to the 7-th order. This huge increase in accuracy by OLTEM compared to that for high-order finite elements is impressive because high-order finite elements have much wider stencils and require a much greater computation time.

To study the convergence and stability of the numerical results for the elliptical interface obtained by OLTEM in more detail, Figure 13 presents the Curves 1 and 2 in Figure 12 at

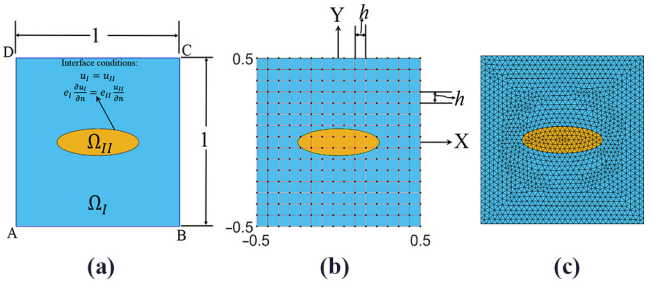

Notes: (a) Examples of a Cartesian mesh; (b) for OLTEM and a mesh with linear triangular finite elements; (c) generated by the commercial software COMSOL

Figure 11. A two-dimensional bi-material plate *ABCD* with a elliptical interface centered at (0, 0)

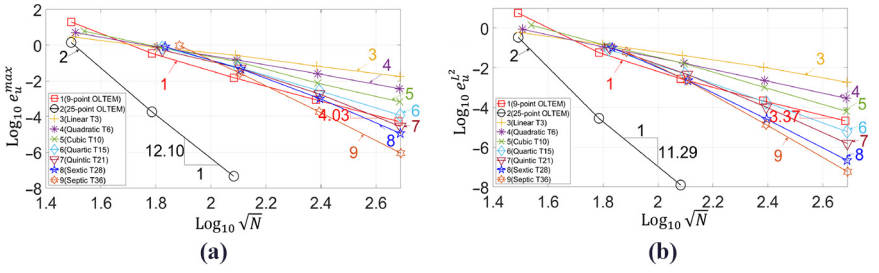

Notes: The numerical solutions of the two-dimensional Poisson equation are obtained by OLTEM with the 9-point (Curve 1) and 25-point (Curve 2) stencils on uniform square (by = 1) Cartesian meshes, as well as by linear and high-order triangular finite elements (Curves 3–9). Curves 3, 4,…,9 correspond to linear, quadratic,…, the 7-th order elements

Figure 12. The maximum relative error e_u^{max} (a) and the L^2 error norm $e_u^{L^2}$ (b) as a function of $\sqrt{N}$ in the logarithmic scale at mesh refinement for the two-dimensional plate with the elliptical interface; N is the number of degrees of freedom

small changes of the Cartesian mesh size h_i (Curve 1 in Figure 13(a) and 13(b) correspond to Curves 2 and 1 in Figure 12(a). For this study, we solve the test problem on 1001 Cartesian meshes with the mesh sizes h_i ($i = 1, 2, \ldots, 1001$) given by equation (35). As can be seen from Figure 13, the errors for OLTEM with the 9-point and 25-point stencils smoothly decrease (with small oscillations) with the decrease in the mesh size h. The small oscillations decrease with the decrease in the mesh size h. This means OLTEM yields stable and convergent numerical results.

4. Concluding remarks

OLTEM for the time-independent Poisson equation with irregular interfaces developed in this paper is the extension of the technique considered in our paper (Idesman and Dey, 2021) for the time-dependent scalar wave and heat equations. Due to the absence of the time variable, the stencil equations, the derivations, as well as the imposition of the interface conditions for OLTEM are different for the Poisson equation compared to those in our paper (Idesman and Dey, 2021) (see also the Introduction). Nevertheless, OLTEM developed for the Poisson equation shares many advantages of OLTEM developed in our paper (Idesman and Dey, 2021) for the time-dependent PDEs. One of the ideas that allows the effective development of the new technique for heterogeneous materials is the addition of the interface conditions at a small number of the interface points to the expression for the local truncation error. The unknown stencil coefficients can be numerically calculated from a small local system of algebraic equations for the general geometry of interfaces. This procedure does not change the width of the stencil equation; i.e. the size of the global discrete system of equations is the same for the Poisson equation with constant or discontinuous coefficients. The calculation of the unknown stencil coefficients is based on the minimization of the local truncation error of the stencil equations and yields the optimal order of accuracy of the new technique at a given stencil width. The increase in the computational costs for the calculation of the unknown stencil coefficients from the local system is insignificant compared to the computational costs for the solution of the global discrete system.

The main advantages of the suggested technique can be summarized as follows:

- Many difficulties of the existing numerical techniques for irregular domains (e.g. finite elements, spectral element, isogeometric elements, the finite volume method and many other) are related to complicated mesh generators for conformed meshes and the accuracy of 'bad' elements (e.g. the elements with small angles). In contrast

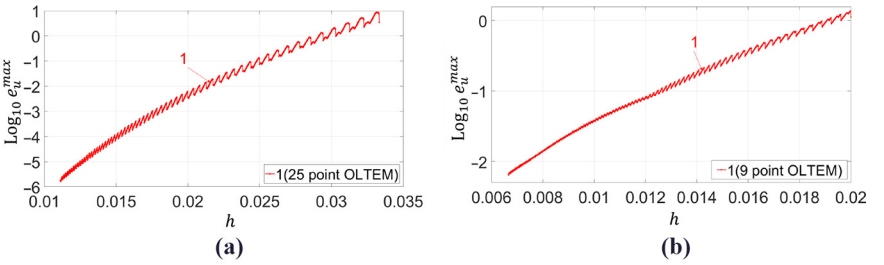

Figure 13.
The logarithm of the maximum relative errors e_u^{max} as a function of the mesh size h for the two-dimensional plate with the elliptical interface [Figure 11(a)]

Notes: The numerical solutions of the two-dimensional Poisson equation are obtained by OLTEM with the 25-point (a) and 9-point (b) stencils on uniform square ($b_y = 1$) Cartesian meshes with the contrast $\frac{c_u}{c_t} = 50$. Each curve is calculated on 1001 meshes

to these techniques, OLTEM is based on trivial unfitted Cartesian meshes with a trivial procedure for the formation of the 9-point and 25-point stencils for two-dimensional domains with complex irregular interfaces.

- The new approach has the same width of the stencil equations and the same structure of the sparse global discrete equations for the Poisson equation with the constant and discontinuous coefficients. There are no unknowns on the interfaces between different materials for the proposed technique; i.e. complex irregular interfaces do not affect the structure of the global system of equations (they affect just the values of the stencils coefficients).
- In contrast to the finite-difference techniques with the stencil coefficients calculated through the approximation of separate partial derivatives, the entire partial differential equation is used for the calculation of the stencil coefficients in OLTEM. This leads to the optimal accuracy of the proposed technique. For example, the 9-point and 25-point stencils of the new two-dimensional approach provide the optimal accuracy that cannot be improved without changing the width of stencil equations. In contrast to the 9-point and 25-point stencils of linear and quadratic quadrilateral finite elements, OLTEM yields a much higher order of accuracy (the increase in accuracy by one order with the 9-point stencils and by eight orders with the 25-point stencils) compared to that for linear and quadratic finite elements for the general geometry of interfaces.
- OLTEM with the 25-point stencils provides a huge increase in accuracy by 8 orders compared to the recent numerical techniques (Zhang and Babuska, 2020; Xiao *et al.*,2020; Guo and Lin, 2019; Cheung *et al.*, 2020) with quadratic elements and unfitted Cartesian meshes. All these techniques including OLTEM have the same structure of sparse global matrices (the difference is only in the values of the matrix coefficients for different techniques).
- The numerical results for irregular interfaces also show that at the same number of degrees of freedom, OLTEM is even much more accurate than high-order (up to the seventh order) finite elements with much wider stencils. This also means that at a given accuracy, OLTEM significantly reduces the computation time compared to that for linear and high-order finite elements.
- OLTEM does not require time consuming numerical integration for finding the coefficients of the stencil equations; for example, as for the high-order finite, spectral and isogeometric elements. The stencil coefficients are calculated analytically or numerically (for the general geometry of interfaces) by the solution of small local systems of linear algebraic equations. Numerical experiments show that the solution of these small local systems of algebraic equations is fast. Moreover, these local systems are independent of each other and can be efficiently solved on a parallel computer.

In the future we plan to extend OLTEM with irregular interfaces to the three-dimensional case. Another direction is the development of OLTEM with adaptive refinement similar to h– and p– refinement for finite elements (e.g. it was shown in papers (Idesman and Dey, 2020a; Idesman and Dey, 2020d) that OLTEM can easily combine different stencils). We plan to use quadtrees/octrees meshes that allow a simple refinement strategy with Cartesian meshes. The extension of OLTEM to other PDEs with discontinuous coefficients, as well as to non-linear PDEs will be also considered in the future.

References

Bathe, K.J. (1996), *Finite Element Procedures*, Prentice-Hall Inc., Upper Saddle River, NJ.

Burman, E. and Hansbo, P. (2010), "Fictitious domain finite element methods using cut elements: I. a stabilized Lagrange multiplier method", *Computer Methods in Applied Mechanics and Engineering*, Vol. 199 Nos 41/44, pp. 2680-2686.

Cheung, J., Gunzburger, M., Bochev, P. and Perego, M. (2020), "An optimally convergent higher-order finite element coupling method for interface and domain decomposition problems", *Results in Applied Mathematics*, Vol. 6, p. 100094.

Coco, A. and Russo, G. (2018), "Second order finite-difference ghost-point multigrid methods for elliptic problems with discontinuous coefficients on an arbitrary interface", *Journal of Computational Physics*, Vol. 361, pp. 299-330.

Crockett, R., Colella, P. and Graves, D. (2011), "A cartesian grid embedded boundary method for solving the Poisson and heat equations with discontinuous coefficients in three dimensions", *Journal of Computational Physics*, Vol. 230 No. 7, pp. 2451-2469.

Dey, B. and Idesman, A. (2020), "A new numerical approach to the solution of PDEs with optimal accuracy on irregular domains and cartesian meshes. Part 2: numerical simulation and comparison with FEM", *Archive of Applied Mechanics*, Vol. 90 No. 12, pp. 2649-2674.

Guittet, A., Lepilliez, M., Tanguy, S. and Gibou, F. (2015), "Solving elliptic problems with discontinuities on irregular domains – the Voronoi interface method", *Journal of Computational Physics*, Vol. 298, pp. 747-765.

Guo, R. and Lin, T. (2019), "A higher degree immersed finite element method based on a Cauchy extension for elliptic interface problems", *SIAM Journal on Numerical Analysis*, Vol. 57 No. 4, pp. 1545-1573.

Guo, R. and Lin, T. (2020), "An immersed finite element method for elliptic interface problems in three dimensions", *Journal of Computational Physics*, Vol. 414, p. 109478.

Gürkan, C. and Massing, A. (2019), "A stabilized cut discontinuous Galerkin framework for elliptic boundary value and interface problems", *Computer Methods in Applied Mechanics and Engineering*, Vol. 348, pp. 466-499.

Idesman, A. (2018), "The use of the local truncation error to improve arbitrary-order finite elements for the linear wave and heat equations", *Computer Methods in Applied Mechanics and Engineering*, Vol. 334, pp. 268-312.

Idesman, A. (2020), "A new numerical approach to the solution of PDEs with optimal accuracy on irregular domains and cartesian meshes. Part 1: the derivations for the wave, heat and Poisson equations in the 1-D and 2-D cases", *Archive of Applied Mechanics*, Vol. 90 No. 12, pp. 2621-2648.

Idesman, A. and Dey, B. (2019), "A new 3-D numerical approach to the solution of PDEs with optimal accuracy on irregular domains and cartesian meshes", *Computer Methods in Applied Mechanics and Engineering*, Vol. 354, pp. 568-592.

Idesman, A. and Dey, B. (2020a), "A new numerical approach to the solution of the 2-D Helmholtz equation with optimal accuracy on irregular domains and cartesian meshes", *Computational Mechanics*, Vol. 65 No. 4, pp. 1189-1204.

Idesman, A. and Dey, B. (2020b), "Accurate numerical solutions of 2-d elastodynamics problems using compact high-order stencils", *Computers and Structures*, Vol. 229, pp. 1-18.

Idesman, A. and Dey, B. (2020c), "Compact high-order stencils with optimal accuracy for numerical solutions of 2-d time-independent elasticity equations", *Computer Methods in Applied Mechanics and Engineering*, Vol. 360, pp. 1-17.

Idesman, A. and Dey, B. (2020d), "New 25-point stencils with optimal accuracy for 2-d heat transfer problems. Comparison with the quadratic isogeometric elements", *Journal of Computational Physics*, Vol. 418, p. 109640.

Idesman, A. and Dey, B. (2020e), "The treatment of the Neumann boundary conditions for a new numerical approach to the solution of PDEs with optimal accuracy on irregular domains and cartesian meshes", *Computer Methods in Applied Mechanics and Engineering*, Vol. 365, p. 112985.

Idesman, A. and Dey, B. (2021), "Optimal local truncation error method for solution of wave and heat equations for heterogeneous materials with irregular interfaces and unfitted cartesian meshes", *Computer Methods in Applied Mechanics and Engineering*, Vol. 384, p. 113998.

Johansen, H. and Colella, P. (1998), "A cartesian grid embedded boundary method for poisson's equation on irregular domains", *Journal of Computational Physics*, Vol. 147 No. 1, pp. 60-85.

Kreiss, H.-O. and Petersson, N.A. (2006), "A second order accurate embedded boundary method for the wave equation with Dirichlet data", *SIAM Journal on Scientific Computing*, Vol. 27 No. 4, pp. 1141-1167.

Kreiss, H.-O., Petersson, N.A. and Ystrom, J. (2004), "Difference approximations of the Neumann problem for the second order wave equation", *SIAM Journal on Numerical Analysis*, Vol. 42 No. 3, pp. 1292-1323.

Kreisst, H.-O. and Petersson, N.A. (2006), "An embedded boundary method for the wave equation with discontinuous coefficients", *SIAM Journal on Scientific Computing*, Vol. 28 No. 6, pp. 2054-2074.

Langtangen, H.P. and Linge, S. (2017), *Finite Difference Computing with PDEs*, Springer.

Li, K., Atallah, N.M., Main, G.A. and Scovazzi, G. (2020), "The shifted interface method: a flexible approach to embedded interface computations", *International Journal for Numerical Methods in Engineering*, Vol. 121 No. 3, pp. 492-518.

McCorquodale, P., Colella, P. and Johansen, H. (2001), "A cartesian grid embedded boundary method for the heat equation on irregular domains", *Journal of Computational Physics*, Vol. 173 No. 2, pp. 620-635.

Main, A. and Scovazzi, G. (2018), "The shifted boundary method for embedded domain computations. part i: Poisson and stokes problems", *Journal of Computational Physics*, Vol. 372, pp. 972-995.

May, S. and Berger, M. (2017), "An explicit implicit scheme for cut cells in embedded boundary meshes", *Journal of Scientific Computing*, Vol. 71 No. 3, pp. 919-943.

Rank, E., Kollmannsberger, S., Sorger, C. and Duster, A. (2011), "Shell finite cell method: a high order fictitious domain approach for thin-walled structures", *Computer Methods in Applied Mechanics and Engineering*, Vol. 200 Nos 45/46, pp. 3200-3209.

Rank, E., Ruess, M., Kollmannsberger, S., Schillinger, D. and Duster, A. (2012), "Geometric modeling, isogeometric analysis and the finite cell method", *Computer Methods in Applied Mechanics and Engineering*, Vol. 249-252, pp. 104-115.

Song, T., Main, A., Scovazzi, G. and Ricchiuto, M. (2018), "The shifted boundary method for hyperbolic systems: embedded domain computations of linear waves and shallow water flows", *Journal of Computational Physics*, Vol. 369, pp. 45-79.

Vallaghe, S. and Papadopoulo, T. (2010), "A trilinear immersed finite element method for solving the electroencephalography forward problem", *SIAM Journal on Scientific Computing*, Vol. 32 No. 4, pp. 2379-2394.

Vos, P., van Loon, R. and Sherwin, S. (2008), "A comparison of fictitious domain methods appropriate for spectral/hp element discretisations", *Computer Methods in Applied Mechanics and Engineering*, Vol. 197 Nos 25/28, pp. 2275-2289.

Xiao, Y., Xu, J. and Wang, F. (2020), "High-order extended finite element methods for solving interface problems", *Computer Methods in Applied Mechanics and Engineering*, Vol. 364, p. 112964.

Zhang, Q. and Babuska, I. (2020), "A stable generalized finite element method (SGFEM) of degree two for interface problems", *Computer Methods in Applied Mechanics and Engineering*, Vol. 363, p. 112889.

Zhang, Q., Ito, K., Li, Z. and Zhang, Z. (2015), "Immersed finite elements for optimal control problems of elliptic PDEs with interfaces", *Journal of Computational Physics*, Vol. 298, pp. 305-319.

Appendix 1. Coefficients bp used in equation (17) for the 9-point stencils

The first ten coefficients b_p ($i = p$, 2,. . ., 10) are presented below. All coefficients b_p (i = 1, 2,. . ., 18) for the 9-point stencils are given in the attached files 'b-coef-9.nb.'

$$b_1 = a_1k_1 + a_2k_2 + a_3k_3 + a_4k_4 + a_5k_5 + a_6k_6 + a_7k_7 + a_8k_8 + a_9k_9 + q_{1,1} + q_{1,2} + q_{1,3} + q_{1,4} + q_{1,5}$$

$$b_2 = -a_1k_1 - a_2k_2 - a_3k_3 - a_4k_4 - a_5k_5 - a_6k_6 - a_7k_7 - a_8k_8 - a_9k_9 + k_1 + k_2 + k_3 + k_4 + k_5 + k_6 + k_7 + k_8 + k_9 - q_{1,1} - q_{1,2} - q_{1,3} - q_{1,4} - q_{1,5}$$

$$\begin{aligned} b_3 = {} & -a_1k_1\left(b_ydy_G + b_y\right) - a_2k_2\left(b_ydy_G + b_y\right) - a_3b_ydy_Gk_3 - a_3b_yk_3 - a_4b_ydy_Gk_4 \\ & - a_5b_ydy_Gk_5 - a_6b_ydy_Gk_6 - a_7b_ydy_Gk_7 + a_7b_yk_7 - a_8b_ydy_Gk_8 + a_8b_yk_8 - a_9b_ydy_Gk_9 \\ & + a_9b_yk_9 + d_{y,2}q_{1,2} + d_{y,3}q_{1,3} + d_{y,4}q_{1,4} + d_{y,5}q_{1,5} + e_*n_{y,1}q_{2,1} + e_*n_{y,2}q_{2,2} + e_*n_{y,3}q_{2,3} \\ & + e_*n_{y,4}q_{2,4} + e_*n_{y,5}q_{2,5} \end{aligned}$$

$$\begin{aligned} b_4 = {} & b_ydy_G((a_1 - 1)k_1 + (a_2 - 1)k_2 + a_3k_3 + a_4k_4 + a_5k_5 + a_6k_6 + a_7k_7 + a_8k_8 \\ & + a_9k_9 - k_3 - k_4 - k_5 - k_6 - k_7 - k_8 - k_9) \\ & + b_y((a_1 - 1)k_1 + (a_2 - 1)k_2 + a_3k_3 - a_7k_7 - a_8k_8 - a_9k_9 - k_3 + k_7 + k_8 + k_9) \\ & - d_{y,2}q_{1,2} - d_{y,3}q_{1,3} - d_{y,4}q_{1,4} - d_{y,5}q_{1,5} - e_{**}n_{y,1}q_{2,1} - e_{**}n_{y,2}q_{2,2} \\ & - e_{**}n_{y,3}q_{2,3} - e_{**}n_{y,4}q_{2,4} - e_{**}n_{y,5}q_{2,5} \end{aligned}$$

$$\begin{aligned} b_5 = {} & -a_1(dx_G + 1)k_1 - a_2dx_Gk_2 - a_3dx_Gk_3 + a_3k_3 - a_4dx_Gk_4 - a_4k_4 - a_5dx_Gk_5 \\ & - a_6dx_Gk_6 + a_6k_6 - a_7dx_Gk_7 - a_7k_7 \\ & - a_8dx_Gk_8 - a_9dx_Gk_9 + a_9k_9 + d_{x,2}q_{1,2} + d_{x,3}q_{1,3} + d_{x,4}q_{1,4} + d_{x,5}q_{1,5} \\ & + e_*n_{x,1}q_{2,1} + e_*n_{x,2}q_{2,2} + e_*n_{x,3}q_{2,3} + e_*n_{x,4}q_{2,4} + e_*n_{x,5}q_{2,5} \end{aligned}$$

$$\begin{aligned} b_6 = {} & (a_1 - 1)(dx_G + 1)k_1 + dx_G((a_2 - 1)k_2 + (a_3 - 1)k_3 + a_4k_4 \\ & + a_5k_5 + a_6k_6 + a_7k_7 + a_8k_8 + a_9k_9 - k_4 - k_5 - k_6 - k_7 - k_8 - k_9) - a_3k_3 + a_4k_4 \\ & - a_6k_6 + a_7k_7 - a_9k_9 - d_{x,2}q_{1,2} - d_{x,3}q_{1,3} - d_{x,4}q_{1,4} - d_{x,5}q_{1,5} - e_{**}n_{x,1}q_{2,1} \\ & - e_{**}n_{x,2}q_{2,2} - e_{**}n_{x,3}q_{2,3} - e_{**}n_{x,4}q_{2,4} - e_{**}n_{x,5}q_{2,5} + k_3 - k_4 + k_6 - k_7 + k_9 \end{aligned}$$

$$
\begin{aligned}
b_7 = \frac{1}{2}(&a_1k_1({b_y}^2{dy_G}^2 + 2b_yb_ydy_G + {b_y}^2 - {dx_G}^2 - 2dx_G - 1) + a_2k_2({b_y}^2{dy_G}^2 + 2b_yb_ydy_G \\
&+{b_y}^2 - {dx_G}^2) + a_3{b_y}^2{dy_G}^2k_3 + 2a_3b_yb_ydy_Gk_3 + a_3{b_y}^2k_3 - a_3{dx_G}^2k_3 + 2a_3dx_Gk_3 - a_3k_3 \\
&+a_4{b_y}^2{dy_G}^2k_4 - a_4{dx_G}^2k_4 - 2a_4dx_Gk_4 - a_4k_4 + a_5{b_y}^2{dy_G}^2k_5 - a_5{dx_G}^2k_5 \\
&+a_6{b_y}^2{dy_G}^2k_6 - a_6{dx_G}^2k_6 + 2a_6dx_Gk_6 - a_6k_6 + a_7{b_y}^2{dy_G}^2k_7 - 2a_7b_yb_ydy_Gk_7 \\
&+a_7{b_y}^2k_7 - a_7{dx_G}^2k_7 - 2a_7dx_Gk_7 - a_7k_7 + a_8{b_y}^2{dy_G}^2k_8 - 2a_8b_yb_ydy_Gk_8 \\
&+a_8{b_y}^2k_8 - a_8{dx_G}^2k_8 + a_9{b_y}^2{dy_G}^2k_9 - 2a_9b_yb_ydy_Gk_9 + a_9{b_y}^2k_9 - a_9{dx_G}^2k_9 + 2a_9dx_Gk_9 \\
&-a_9k_9 - d_{x,2}^2q_{1,2} - 2d_{x,2}e_*n_{x,2}q_{2,2} + d_{y,2}^2q_{1,2} + 2d_{y,2}e_*n_{y,2}q_{2,2} \\
&-d_{x,3}^2q_{1,3} - 2d_{x,3}e_*n_{x,3}q_{2,3} + d_{y,3}^2q_{1,3} + 2d_{y,3}e_*n_{y,3}q_{2,3} - d_{x,4}^2q_{1,4} - 2d_{x,4}e_*n_{x,4}q_{2,4} \\
&+d_{y,4}^2q_{1,4} + 2d_{y,4}e_*n_{y,4}q_{2,4} - d_{x,5}^2q_{1,5} \\
&-2d_{x,5}e_*n_{x,5}q_{2,5} + d_{y,5}^2q_{1,5} + 2d_{y,5}e_*n_{y,5}q_{2,5})
\end{aligned}
$$

$$
\begin{aligned}
b_8 = \frac{1}{2}(&-(a_1-1)k_1({b_y}^2{dy_G}^2 + 2b_yb_ydy_G + {b_y}^2 - {dx_G}^2 - 2dx_G - 1) - 2b_yb_ydy_G((a_2-1)k_2 \\
&+(a_3-1)k_3 - a_7k_7 - a_8k_8 - a_9k_9 + k_7 + k_8 + k_9) + {b_y}^2(-a_2k_2 - a_3k_3 - a_7k_7 - a_8k_8 \\
&-a_9k_9 + k_2 + k_3 + k_7 + k_8 + k_9) - a_2{b_y}^2{dy_G}^2k_2 + a_2{dx_G}^2k_2 - a_3{b_y}^2{dy_G}^2k_3 \\
&+a_3{dx_G}^2k_3 - 2a_3dx_Gk_3 + a_3k_3 - a_4{b_y}^2{dy_G}^2k_4 + a_4{dx_G}^2k_4 + 2a_4dx_Gk_4 \\
&+a_4k_4 - a_5{b_y}^2{dy_G}^2k_5 + a_5{dx_G}^2k_5 - a_6{b_y}^2{dy_G}^2k_6 + a_6{dx_G}^2k_6 - 2a_6dx_Gk_6 \\
&+a_6k_6 - a_7{b_y}^2{dy_G}^2k_7 + a_7{dx_G}^2k_7 + 2a_7dx_Gk_7 + a_7k_7 - a_8{b_y}^2{dy_G}^2k_8 + a_8{dx_G}^2k_8 - a_9{b_y}^2{dy_G}^2k_9 \\
&+a_9{dx_G}^2k_9 - 2a_9dx_Gk_9 + a_9k_9 + {b_y}^2{dy_G}^2k_2 + {b_y}^2{dy_G}^2k_3 + {b_y}^2{dy_G}^2k_4 + {b_y}^2{dy_G}^2k_5 \\
&+{b_y}^2{dy_G}^2k_6 + {b_y}^2{dy_G}^2k_7 + {b_y}^2{dy_G}^2k_8 + {b_y}^2{dy_G}^2k_9 + d_{x,2}^2q_{1,2} + 2d_{x,2}e_{**}n_{x,2}q_{2,2} \\
&-d_{y,2}^2q_{1,2} - 2d_{y,2}e_{**}n_{y,2}q_{2,2} + d_{x,3}^2q_{1,3} + 2d_{x,3}e_{**}n_{x,3}q_{2,3} - d_{y,3}^2q_{1,3} \\
&-2d_{y,3}e_{**}n_{y,3}q_{2,3} + d_{x,4}^2q_{1,4} + 2d_{x,4}e_{**}n_{x,4}q_{2,4} - d_{y,4}^2q_{1,4} - 2d_{y,4}e_{**}n_{y,4}q_{2,4} + d_{x,5}^2q_{1,5} \\
&+2d_{x,5}e_{**}n_{x,5}q_{2,5} - d_{y,5}^2q_{1,5} - 2d_{y,5}e_{**}n_{y,5}q_{2,5} - dx_G{}^2k_2 - dx_G{}^2k_3 - dx_G{}^2k_4 \\
&-dx_G{}^2k_5 - dx_G{}^2k_6 - dx_G{}^2k_7 - dx_G{}^2k_8 - dx_G{}^2k_9 + 2dx_Gk_3 - 2dx_Gk_4 \\
&+2dx_Gk_6 - 2dx_Gk_7 + 2dx_Gk_9 - k_3 - k_4 - k_6 - k_7 - k_9)
\end{aligned}
$$

$$
\begin{aligned}
b_9 = {} & a_1(dx_G+1)k_1\big(b_ydy_G + b_y\big) + a_2dx_Gk_2\big(b_ydy_G + b_y\big) + a_3b_ydx_Gdy_Gk_3 - a_3b_ydy_Gk_3 \\
& + a_3b_ydx_Gk_3 - a_3b_yk_3 + a_4b_ydx_Gdy_Gk_4 + a_4b_ydy_Gk_4 + a_5b_ydx_Gdy_Gk_5 + a_6b_ydx_Gdy_Gk_6 \\
& - a_6b_ydy_Gk_6 + a_7b_ydx_Gdy_Gk_7 + a_7b_ydy_Gk_7 - a_7b_ydx_Gk_7 - a_7b_yk_7 + a_8b_ydx_Gdy_Gk_8 \\
& - a_8b_ydx_Gk_8 + a_9b_ydx_Gdy_Gk_9 - a_9b_ydy_Gk_9 - a_9b_ydx_Gk_9 + a_9b_yk_9 + d_{x,2}d_{y,2}q_{1,2} \\
& + d_{x,2}e_*n_{y,2}q_{2,2} + d_{y,2}e_*n_{x,2}q_{2,2} + d_{x,3}d_{y,3}q_{1,3} + d_{x,3}e_*n_{y,3}q_{2,3} + d_{y,3}e_*n_{x,3}q_{2,3} + d_{x,4}d_{y,4}q_{1,4} \\
& + d_{x,4}e_*n_{y,4}q_{2,4} + d_{y,4}e_*n_{x,4}q_{2,4} + d_{x,5}d_{y,5}q_{1,5} + d_{x,5}e_*n_{y,5}q_{2,5} + d_{y,5}e_*n_{x,5}q_{2,5}
\end{aligned}
$$

$$
\begin{aligned}
b_{10} = {} & b_ydy_G\big(-(a_1-1)(dx_G+1)k_1 + dx_G(-a_2k_2 - a_3k_3 - a_4k_4 - a_5k_5 - a_6k_6 - a_7k_7 \\
& -a_8k_8 - a_9k_9 + k_2 + k_3 + k_4 + k_5 + k_6 + k_7 + k_8 + k_9) + a_3k_3 - a_4k_4 + a_6k_6 \\
& -a_7k_7 + a_9k_9 - k_3 + k_4 - k_6 + k_7 - k_9) + b_y\big(-(a_1-1)(dx_G+1)k_1 + dx_G(-a_2k_2 - a_3k_3 \\
& +a_7k_7 + a_8k_8 + a_9k_9 + k_2 + k_3 - k_7 - k_8 - k_9) + a_3k_3 + a_7k_7 - a_9k_9 - k_3 - k_7 + k_9) \\
& -d_{x,2}d_{y,2}q_{1,2} - d_{x,2}e_{**}n_{y,2}q_{2,2} - d_{y,2}e_{**}n_{x,2}q_{2,2} - d_{x,3}d_{y,3}q_{1,3} - d_{x,3}e_{**}n_{y,3}q_{2,3} \\
& -d_{y,3}e_{**}n_{x,3}q_{2,3} - d_{x,4}d_{y,4}q_{1,4} - d_{x,4}e_{**}n_{y,4}q_{2,4} - d_{y,4}e_{**}n_{x,4}q_{2,4} \\
& -d_{x,5}d_{y,5}q_{1,5} - d_{x,5}e_{**}n_{y,5}q_{2,5} - d_{y,5}e_{**}n_{x,5}q_{2,5}
\end{aligned}
$$

Appendix 2. Coefficients kj (j = 1, 2,. . ., 25) for homogeneous materials with the 25-point uniform stencils

$$k_1 = \frac{\left(b_y{}^2+1\right)^2\left(176656b_y{}^{12}-185512b_y{}^{10}-2284531b_y{}^8+4579274b_y{}^6-2284531b_y{}^4-185512b_y{}^2+176656\right)}{36\left(58288976b_y{}^{16}-12041600b_y{}^{14}-1112834229b_y{}^{12}+805729100b_y{}^{10}+7325265506b_y{}^8+805729100b_y{}^6-1112834229b_y{}^4-12041600b_y{}^2+58288976\right)},$$

$$k_2 = -\frac{4\left(44164b_y{}^{16}-911975b_y{}^{14}+280624b_y{}^{12}+12099950b_y{}^{10}-25914856b_y{}^8+6967025b_y{}^6+26422684b_y{}^4-14930000b_y{}^2+2392384\right)}{9\left(58288976b_y{}^{16}-12041600b_y{}^{14}-1112834229b_y{}^{12}+805729100b_y{}^{10}+7325265506b_y{}^8+805729100b_y{}^6-1112834229b_y{}^4-12041600b_y{}^2+58288976\right)},$$

$$k_3 = \frac{176656b_y{}^{16}-4919800b_y{}^{14}+83309881b_y{}^{12}-441576750b_y{}^{10}+1159844496b_y{}^8-1756955850b_y{}^6+1456399991b_y{}^4-481727600b_y{}^2+58288976}{6\left(58288976b_y{}^{16}-12041600b_y{}^{14}-1112834229b_y{}^{12}+805729100b_y{}^{10}+7325265506b_y{}^8+805729100b_y{}^6-1112834229b_y{}^4-12041600b_y{}^2+58288976\right)},$$

$$k_4 = -\frac{4\left(44164b_y{}^{16}-911975b_y{}^{14}+280624b_y{}^{12}+12099950b_y{}^{10}-25914856b_y{}^8+6967025b_y{}^6+26422684b_y{}^4-14930000b_y{}^2+2392384\right)}{9\left(58288976b_y{}^{16}-12041600b_y{}^{14}-1112834229b_y{}^{12}+805729100b_y{}^{10}+7325265506b_y{}^8+805729100b_y{}^6-1112834229b_y{}^4-12041600b_y{}^2+58288976\right)},$$

$$k_5 = \frac{\left(b_y{}^2+1\right)^2\left(176656b_y{}^{12}-185512b_y{}^{10}-2284531b_y{}^8+4579274b_y{}^6-2284531b_y{}^4-185512b_y{}^2+176656\right)}{36\left(58288976b_y{}^{16}-12041600b_y{}^{14}-1112834229b_y{}^{12}+805729100b_y{}^{10}+7325265506b_y{}^8+805729100b_y{}^6-1112834229b_y{}^4-12041600b_y{}^2+58288976\right)},$$

$$k_6 = -\frac{4\left(2392384b_y{}^{16}-14930000b_y{}^{14}+26422684b_y{}^{12}+6967025b_y{}^{10}-25914856b_y{}^8+12099950b_y{}^6+280624b_y{}^4-911975b_y{}^2+44164\right)}{9\left(58288976b_y{}^{16}-12041600b_y{}^{14}-1112834229b_y{}^{12}+805729100b_y{}^{10}+7325265506b_y{}^8+805729100b_y{}^6-1112834229b_y{}^4-12041600b_y{}^2+58288976\right)},$$

$$k_7 = \frac{16\left(2392384b_y{}^{16}-14997200b_y{}^{14}-178436b_y{}^{12}+228722825b_y{}^{10}-597576646b_y{}^8+228722825b_y{}^6-178436b_y{}^4-14997200b_y{}^2+2392384\right)}{9\left(58288976b_y{}^{16}-12041600b_y{}^{14}-1112834229b_y{}^{12}+805729100b_y{}^{10}+7325265506b_y{}^8+805729100b_y{}^6-1112834229b_y{}^4-12041600b_y{}^2+58288976\right)},$$

$$k_8 = -\frac{8\left(2392384b_y{}^{16}-15019600b_y{}^{14}+99039004b_y{}^{12}-372886575b_y{}^{10}+3695355584b_y{}^8-685156950b_y{}^6-220654216b_y{}^4-32365775b_y{}^2+14572244\right)}{3\left(58288976b_y{}^{16}-12041600b_y{}^{14}-1112834229b_y{}^{12}+805729100b_y{}^{10}+7325265506b_y{}^8+805729100b_y{}^6-1112834229b_y{}^4-12041600b_y{}^2+58288976\right)},$$

$$k_9 = \frac{16\left(2392384b_y{}^{16}-14997200b_y{}^{14}-178436b_y{}^{12}+228722825b_y{}^{10}-597576646b_y{}^8+228722825b_y{}^6-178436b_y{}^4-14997200b_y{}^2+2392384\right)}{9\left(58288976b_y{}^{16}-12041600b_y{}^{14}-1112834229b_y{}^{12}+805729100b_y{}^{10}+7325265506b_y{}^8+805729100b_y{}^6-1112834229b_y{}^4-12041600b_y{}^2+58288976\right)},$$

$$k_{10} = -\frac{4\left(2392384b_y{}^{16}-14930000b_y{}^{14}+26422684b_y{}^{12}+6967025b_y{}^{10}-25914856b_y{}^8+12099950b_y{}^6+280624b_y{}^4-911975b_y{}^2+44164\right)}{9\left(58288976b_y{}^{16}-12041600b_y{}^{14}-1112834229b_y{}^{12}+805729100b_y{}^{10}+7325265506b_y{}^8+805729100b_y{}^6-1112834229b_y{}^4-12041600b_y{}^2+58288976\right)},$$

$$k_{11} = \frac{58288976b_y{}^{16}-481727600b_y{}^{14}+1456399991b_y{}^{12}-1756955850b_y{}^{10}+1159844496b_y{}^8-441576750b_y{}^6+83309881b_y{}^4-4919800b_y{}^2+176656}{6\left(58288976b_y{}^{16}-12041600b_y{}^{14}-1112834229b_y{}^{12}+805729100b_y{}^{10}+7325265506b_y{}^8+805729100b_y{}^6-1112834229b_y{}^4-12041600b_y{}^2+58288976\right)},$$

$$k_{12} = -\frac{8\left(14572244b_y{}^{16}-32365775b_y{}^{14}-220654216b_y{}^{12}+685156950b_y{}^{10}+3695355584b_y{}^8-372886575b_y{}^6+99039004b_y{}^4-15019600b_y{}^2+2392384\right)}{3\left(58288976b_y{}^{16}-12041600b_y{}^{14}-1112834229b_y{}^{12}+805729100b_y{}^{10}+7325265506b_y{}^8+805729100b_y{}^6-1112834229b_y{}^4-12041600b_y{}^2+58288976\right)},$$

$$k_{13} = 1,$$

$$k_{14} = -\frac{8\left(14572244b_y^{16} - 3236775b_y^{14} - 220654216b_y^{12} + 685156950b_y^{10} + 369535584b_y^8 - 372886575b_y^6 + 99039004b_y^4 - 15019600b_y^2 + 2392384\right)}{3\left(58288976b_y^{16} - 12041600b_y^{14} - 1112834229b_y^{12} + 805729100b_y^{10} + 7325265506b_y^8 + 805729100b_y^6 - 1112834229b_y^4 - 12041600b_y^2 + 58288976\right)},$$

$$k_{15} = \frac{58288976b_y^{16} - 4817276000b_y^{14} + 1456399991b_y^{12} - 1756955850b_y^{10} + 1159844496b_y^8 - 441576750b_y^6 + 83309881b_y^4 - 4919800b_y^2 + 176656}{6\left(58288976b_y^{16} - 12041600b_y^{14} - 1112834229b_y^{12} + 805729100b_y^{10} + 7325265506b_y^8 + 805729100b_y^6 - 1112834229b_y^4 - 12041600b_y^2 + 58288976\right)},$$

$$k_{16} = -\frac{4\left(2392384b_y^{16} - 14930000b_y^{14} + 26422684b_y^{12} + 6967025b_y^{10} - 25914856b_y^8 + 12099950b_y^6 + 280624b_y^4 - 911975b_y^2 + 44164\right)}{9\left(58288976b_y^{16} - 12041600b_y^{14} - 1112834229b_y^{12} + 805729100b_y^{10} + 7325265506b_y^8 + 805729100b_y^6 - 1112834229b_y^4 - 12041600b_y^2 + 58288976\right)},$$

$$k_{17} = \frac{16\left(2392384b_y^{16} - 14997200b_y^{14} - 178436b_y^{12} + 228722825b_y^{10} - 597576646b_y^8 + 228722825b_y^6 - 178436b_y^4 - 14997200b_y^2 + 2392384\right)}{9\left(58288976b_y^{16} - 12041600b_y^{14} - 1112834229b_y^{12} + 805729100b_y^{10} + 7325265506b_y^8 + 805729100b_y^6 - 1112834229b_y^4 - 12041600b_y^2 + 58288976\right)},$$

$$k_{18} = -\frac{8\left(2392384b_y^{16} - 15019600b_y^{14} + 99039004b_y^{12} - 372886575b_y^{10} + 369535584b_y^8 + 685156950b_y^6 - 220654216b_y^4 - 32365775b_y^2 + 14572244\right)}{3\left(58288976b_y^{16} - 12041600b_y^{14} - 1112834229b_y^{12} + 805729100b_y^{10} + 7325265506b_y^8 + 805729100b_y^6 - 1112834229b_y^4 - 12041600b_y^2 + 58288976\right)},$$

$$k_{19} = \frac{16\left(2392384b_y^{16} - 14997200b_y^{14} - 178436b_y^{12} + 228722825b_y^{10} - 597576646b_y^8 + 228722825b_y^6 - 178436b_y^4 - 14997200b_y^2 + 2392384\right)}{9\left(58288976b_y^{16} - 12041600b_y^{14} - 1112834229b_y^{12} + 805729100b_y^{10} + 7325265506b_y^8 + 805729100b_y^6 - 1112834229b_y^4 - 12041600b_y^2 + 58288976\right)},$$

$$k_{20} = -\frac{4\left(2392384b_y^{16} - 14930000b_y^{14} + 26422684b_y^{12} + 6967025b_y^{10} - 25914856b_y^8 + 12099950b_y^6 + 280624b_y^4 - 911975b_y^2 + 44164\right)}{9\left(58288976b_y^{16} - 12041600b_y^{14} - 1112834229b_y^{12} + 805729100b_y^{10} + 7325265506b_y^8 + 805729100b_y^6 - 1112834229b_y^4 - 12041600b_y^2 + 58288976\right)},$$

$$k_{21} = \frac{\left(b_y^2 + 1\right)^2\left(176656b_y^{12} - 185512b_y^{10} - 2284531b_y^8 + 4579274b_y^6 - 2284531b_y^4 - 185512b_y^2 + 176656\right)}{36\left(58288976b_y^{16} - 12041600b_y^{14} - 1112834229b_y^{12} + 805729100b_y^{10} + 7325265506b_y^8 + 805729100b_y^6 - 1112834229b_y^4 - 12041600b_y^2 + 58288976\right)},$$

$$k_{22} = -\frac{4\left(44164b_y^{16} - 911975b_y^{14} + 280624b_y^{12} + 12099950b_y^{10} - 25914856b_y^8 + 6967025b_y^6 + 26422684b_y^4 - 14930000b_y^2 + 2392384\right)}{9\left(58288976b_y^{16} - 12041600b_y^{14} - 1112834229b_y^{12} + 805729100b_y^{10} + 7325265506b_y^8 + 805729100b_y^6 - 1112834229b_y^4 - 12041600b_y^2 + 58288976\right)},$$

$$k_{23} = \frac{176656b_y^{16} - 4919800b_y^{14} + 83309881b_y^{12} - 441576750b_y^{10} + 1159844496b_y^8 - 1756955850b_y^6 + 1456399991b_y^4 - 481727600b_y^2 + 58288976}{6\left(58288976b_y^{16} - 12041600b_y^{14} - 1112834229b_y^{12} + 805729100b_y^{10} + 7325265506b_y^8 + 805729100b_y^6 - 1112834229b_y^4 - 12041600b_y^2 + 58288976\right)},$$

$$k_{24} = -\frac{4\left(44164b_y^{16} - 911975b_y^{14} + 280624b_y^{12} + 12099950b_y^{10} - 25914856b_y^8 + 6967025b_y^6 + 26422684b_y^4 - 14930000b_y^2 + 2392384\right)}{9\left(58288976b_y^{16} - 12041600b_y^{14} - 1112834229b_y^{12} + 805729100b_y^{10} + 7325265506b_y^8 + 805729100b_y^6 - 1112834229b_y^4 - 12041600b_y^2 + 58288976\right)},$$

$$k_{25} = \frac{\left(b_y^2 + 1\right)^2\left(176656b_y^{12} - 185512b_y^{10} - 2284531b_y^8 + 4579274b_y^6 - 2284531b_y^4 - 185512b_y^2 + 176656\right)}{36\left(58288976b_y^{16} - 12041600b_y^{14} - 1112834229b_y^{12} + 805729100b_y^{10} + 7325265506b_y^8 + 805729100b_y^6 - 1112834229b_y^4 - 12041600b_y^2 + 58288976\right)},$$

Appendix 3. Explicit expression for the term $\overline{f}$ in equation (30) in the case of nonzero source term fl $\neq$ 0 in the Poisson equation

The expression for $\overline{f}$ up to the fourth-order with respect to **h**:

$$
\begin{aligned}
&\overline{f} = \frac{1}{2}((q_{1,2}d_{x,2}^2 + a_1(dx_G+1)^2k_1 + a_3k_3 + a_4k_4 + a_6k_6 + a_7k_7 + a_9k_9 + dx_G(dx_G(a_2k_2\\
&+a_3k_3 + a_4k_4 + a_5k_5 + a_6k_6 + a_7k_7 + a_8k_8 + a_9k_9) - 2(a_3k_3 - a_4k_4 + a_6k_6 - a_7k_7 + a_9k_9)))\\
&+2d_{x,5}e_*n_{x,5}q_{2,5} + d_{x,3}^2q_{1,3} + d_{x,4}^2q_{1,4} + d_{x,5}^2q_{1,5} + 2e_*(d_{x,2}n_{x,2}q_{2,2} + d_{x,3}n_{x,3}q_{2,3} + d_{x,4}n_{x,4}q_{2,4}))\\
&(\tilde{f}_G^*) + (-q_{1,2}d_{x,2}^2 - (a_1-1)(dx_G+1)^2k_1 - a_3k_3 + k_3 - a_4k_4 + k_4 - a_6k_6 + k_6 - a_7k_7\\
&+k_7 - a_9k_9 + k_9 + dx_G(2((a_3-1)k_3 - a_4k_4 + k_4 + (a_6-1)k_6 - a_7k_7 + k_7 + (a_9-1)k_9)\\
&+dx_G(-a_2k_2 + k_2 - a_3k_3 + k_3 - a_4k_4 + k_4 - a_5k_5 + k_5 - a_6k_6 + k_6 - a_7k_7 + k_7 - a_8k_8\\
&+k_8 - a_9k_9 + k_9)) - 2d_{x,5}e_{**}n_{x,5}q_{2,5} - d_{x,3}^2q_{1,3} - d_{x,4}^2q_{1,4} - d_{x,5}^2q_{1,5} - 2e_{**}(d_{x,2}n_{x,2}q_{2,2}\\
&+d_{x,3}n_{x,3}q_{2,3} + d_{x,4}n_{x,4}q_{2,4}))(\tilde{f}_G^{**}))\mathbf{h}^2 + \frac{1}{6}(3(d_{y,2}q_{1,2}d_{x,2}^2 + e_*n_{y,2}q_{2,2}d_{x,2}^2 + 2d_{y,2}e_*n_{x,2}q_{2,2}d_{x,2}\\
&-a_1b_y(dx_G+1)^2(dy_G+1)k_1 - a_2b_ydx_G^2(dy_G+1)k_2 - b_y(a_3(dy_G+1)k_3(dx_G-1)^2\\
&+a_9(dy_G-1)k_9(dx_G-1)^2 + a_4(dx_G+1)^2dy_Gk_4 + a_5dx_G^2dy_Gk_5 + a_6dx_G^2dy_Gk_6\\
&+a_6dy_Gk_6 - 2a_6dx_Gdy_Gk_6 - a_7dx_G^2k_7 - a_7k_7 - 2a_7dx_Gk_7 + a_7dx_G^2dy_Gk_7 + a_7dy_Gk_7\\
&+2a_7dx_Gdy_Gk_7 - a_8dx_G^2k_8 + a_8dx_G^2dy_Gk_8) + 2d_{x,5}d_{y,5}e_*n_{x,5}q_{2,5} + d_{x,5}^2e_*n_{y,5}q_{2,5}\\
&+d_{x,3}^2d_{y,3}q_{1,3} + d_{x,4}^2d_{y,4}q_{1,4} + d_{x,5}^2d_{y,5}q_{1,5} + 2d_{x,3}d_{y,3}e_*n_{x,3}q_{2,3}\\
&+d_{x,3}^2e_*n_{y,3}q_{2,3} + d_{x,4}e_*(2d_{y,4}n_{x,4} + d_{x,4}n_{y,4})q_{2,4})(\tilde{f}_G^*)^{(0,1)} + 3(-d_{y,2}q_{1,2}d_{x,2}^2\\
&+b_y(((a_2-1)(dy_G+1)k_2 + (a_3-1)(dy_G+1)k_3 - a_7k_7 + k_7 - a_8k_8\\
&+k_8 - a_9k_9 + k_9 + dy_G((a_4-1)k_4 + (a_5-1)k_5 + (a_6-1)k_6 + (a_7-1)k_7 + (a_8-1)k_8\\
&+(a_9-1)k_9))dx_G^2 + 2(-(a_3-1)(dy_G+1)k_3 - a_7k_7 + k_7 + (a_9-1)k_9 + dy_G((a_4-1)k_4 - a_6k_6\\
&+k_6 + (a_7-1)k_7 - a_9k_9 + k_9))dx_G + (a_1-1)(dx_G+1)^2(dy_G+1)k_1 + (a_3-1)k_3 - a_7k_7\\
&+(a_9-1)k_9)) - 2d_{x,5}d_{y,5}e_{**}n_{x,5}q_{2,5} - d_{x,3}^2d_{y,3}q_{1,3} - d_{x,4}^2d_{y,4}q_{1,4} - d_{x,5}^2(e_{**}n_{y,5}q_{2,5}\\
&+d_{y,5}q_{1,5}) - e_{**}(d_{x,2}(2d_{y,2}n_{x,2} + d_{x,2}n_{y,2})q_{2,2} + d_{x,3}(2d_{y,3}n_{x,3} + d_{x,3}n_{y,3})q_{2,3}\\
&+d_{x,4}(2d_{y,4}n_{x,4} + d_{x,4}n_{y,4})q_{2,4}))(\tilde{f}_G^{**})^{(0,1)} + (q_{1,2}d_{x,2}^3 - a_1(dx_G+1)^3k_1 + a_3k_3 - a_4k_4\\
&+a_6k_6 - a_7k_7 + a_9k_9 - dx_G(3(a_3k_3 + a_4k_4 + a_6k_6 + a_7k_7 + a_9k_9)\\
&+dx_G(dx_G(a_2k_2 + a_3k_3 + a_4k_4 + a_5k_5 + a_6k_6 + a_7k_7 + a_8k_8 + a_9k_9) - 3(a_3k_3 - a_4k_4\\
&+a_6k_6 - a_7k_7 + a_9k_9))) + 3d_{x,5}^2e_*n_{x,5}q_{2,5} + d_{x,3}^3q_{1,3} + d_{x,4}^3q_{1,4} + d_{x,5}^3q_{1,5} + 3e_*(n_{x,2}q_{2,2}d_{x,2}^2\\
&+d_{x,3}^2n_{x,3}q_{2,3} + d_{x,4}^2n_{x,4}q_{2,4}))(\tilde{f}_G^*)^{(1,0)} + (-q_{1,2}d_{x,2}^3 + (a_1-1)(dx_G+1)^3k_1 - a_3k_3 + k_3\\
&+(a_4-1)k_4 - a_6k_6 + k_6 + (a_7-1)k_7 - a_9k_9 + k_9 + dx_G(((a_2-1)k_2 + (a_3-1)k_3\\
&+(a_4-1)k_4 + (a_5-1)k_5 + (a_6-1)k_6 + (a_7-1)k_7 + (a_8-1)k_8 + (a_9-1)k_9)dx_G^2\\
&-3((a_3-1)k_3 - a_4k_4 + k_4 + (a_6-1)k_6 - a_7k_7 + k_7 + (a_9-1)k_9)dx_G + 3((a_3-1)k_3\\
&+(a_4-1)k_4 + (a_6-1)k_6 + (a_7-1)k_7 + (a_9-1)k_9)) - 3d_{x,5}^2e_{**}n_{x,5}q_{2,5} - d_{x,3}^3q_{1,3}\\
&-d_{x,4}^3q_{1,4} - d_{x,5}^3q_{1,5} - 3e_{**}(n_{x,2}q_{2,2}d_{x,2}^2 + d_{x,3}^2n_{x,3}q_{2,3} + d_{x,4}^2n_{x,4}q_{2,4}))(\tilde{f}_G^{**})^{(1,0)})\mathbf{h}^3\\
&+\Big\{\frac{1}{24}((-q_{1,2}d_{x,2}^4 - 4e_*n_{x,2}q_{2,2}d_{x,2}^3 + 6d_{y,2}q_{1,2}d_{x,2}^2 + 12d_{y,2}e_*n_{y,2}q_{2,2}d_{x,2}^2 + 12d_{y,2}^2e_*n_{x,2}q_{2,2}d_{x,2} - a_1(dx_G+1)^2((dx_G+1)^2\\
&-6b_y^2(dy_G+1)^2)k_1 + a_2dx_G^2(6b_y^2(dy_G+1)^2 - dx_G^2)k_2 - a_3dx_G^4k_3 + 4a_3dx_G^3k_3 + 6a_3b_y^2k_3 + 6a_3b_y^2dx_G^2k_3 - 6a_3dx_G^2k_3\\
&+6a_3b_y^2dy_G^2k_3 + 6a_3b_y^2dx_G^2dy_G^2k_3 - 12a_3b_y^2dx_Gdy_G^2k_3 - a_3k_3 - 12a_3b_y^2dx_Gk_3 + 4a_3dx_Gk_3 + 12a_3b_y^2dy_Gk_3\\
&+12a_3b_y^2dx_G^2dy_Gk_3 - 24a_3b_y^2dx_Gdy_Gk_3 - a_4dx_G^4k_4 - 4a_4dx_G^3k_4 - 6a_4dx_G^2k_4 + 6a_4b_y^2dy_G^2k_4 + 6a_4b_y^2dx_G^2dy_G^2k_4\\
&+12a_4b_y^2dx_Gdy_G^2k_4 - a_4k_4 - 4a_4dx_Gk_4 - a_5dx_G^4k_5 + 6a_5b_y^2dx_G^2dy_G^2k_5 - a_6dx_G^4k_6 + 4a_6dx_G^3k_6 - 6a_6dx_G^2k_6\\
&+6a_6b_y^2dy_G^2k_6 + 6a_6b_y^2dx_G^2dy_G^2k_6 - 12a_6b_y^2dx_Gdy_G^2k_6 - a_6k_6 + 4a_6dx_Gk_6 - a_7dx_G^4k_7 - 4a_7dx_G^3k_7 + 6a_7b_y^2k_7\\
&+6a_7b_y^2dx_G^2k_7 - 6a_7dx_G^2k_7 + 6a_7b_y^2dy_G^2k_7 + 6a_7b_y^2dx_G^2dy_G^2k_7 + 12a_7b_y^2dx_Gdy_G^2k_7 - a_7k_7 + 12a_7b_y^2dx_Gk_7\\
&-4a_7dx_Gk_7 - 12a_7b_y^2dy_Gk_7 - 12a_7b_y^2dx_G^2dy_Gk_7 - 24a_7b_y^2dx_Gdy_Gk_7 - a_8dx_G^4k_8 + 6a_8b_y^2dx_G^2k_8 + 6a_8b_y^2dx_G^2dy_G^2k_8\\
&-12a_8b_y^2dx_G^2dy_Gk_8 - a_9k_9 + a_9(6b_y^2(dx_G-1)^2(dy_G-1)^2 - (dx_G-2)dx_G((dx_G-2)dx_G+2))k_9 - 4d_{x,5}^3e_*n_{x,5}q_{2,5}\\
&+12d_{x,5}d_{y,5}^2e_*n_{x,5}q_{2,5} + 12d_{x,5}^2d_{y,5}e_*n_{y,5}q_{2,5} - d_{x,3}^4q_{1,3} + 6d_{x,3}^2d_{y,3}^2q_{1,3} - d_{x,4}^4q_{1,4} + 6d_{x,4}^2d_{y,4}^2q_{1,4} - d_{x,5}^4q_{1,5} + 6d_{x,5}^2d_{y,5}^2q_{1,5}\\
&-4d_{x,3}^3e_*n_{x,3}q_{2,3} + 12d_{x,3}d_{y,3}^2e_*n_{x,3}q_{2,3} + 12d_{x,3}^2d_{y,3}e_*n_{y,3}q_{2,3} + 4d_{x,4}e_*(-n_{x,4}d_{x,4}^2 + 3d_{y,4}n_{y,4}d_{x,4} + 3d_{y,4}^2n_{x,4})q_{2,4})(\tilde{f}_G^*)^{(0,2)}\\
&+(q_{1,2}d_{x,2}^4 - 6d_{y,2}^2q_{1,2}d_{x,2}^2 + (a_1-1)(dx_G+1)^2((dx_G+1)^2 - 6b_y^2(dy_G+1)^2)k_1 + (a_3-1)k_3 + (a_4-1)k_4 + (a_6-1)\\
&k_6 + (a_7-1)k_7 + (a_9-1)k_9 + dx_G(((a_2-1)k_2 + (a_3-1)k_3 + (a_4-1)k_4 + (a_5-1)k_5 + (a_6-1)k_6 + (a_7-1)k_7 + (a_8-1)k_8
\end{aligned}
$$

$$
\begin{aligned}
&+(a_9-1)k_9)dx_G{}^3-4((a_3-1)k_3-a_4k_4+k_4+(a_6-1)k_6-a_7k_7+k_7+(a_9-1)k_9)dx_G{}^2+6((a_3-1)k_3+(a_4-1)\\
&k_4+(a_6-1)k_6+(a_7-1)k_7+(a_9-1)k_9)dx_G-4((a_3-1)k_3-a_4k_4+k_4+(a_6-1)k_6-a_7k_7+k_7+(a_9-1)k_9))\\
&-6b_y{}^2(((a_2-1)k_2(dy_G+1)^2+(a_3-1)k_3(dy_G+1)^2+(a_7-1)k_7+(a_8-1)k_8+(a_9-1)k_9+dy_G(dy_G((a_4-1)k_4\\
&+(a_5-1)k_5+(a_6-1)k_6+(a_7-1)k_7+(a_8-1)k_8+(a_9-1)k_9)+2(-a_7k_7+k_7-a_8k_8+k_8-a_9k_9+k_9)))dx_G{}^2\\
&+2(((a_4-1)k_4-a_6k_6+k_6+(a_7-1)k_7-a_9k_9+k_9)dy_G{}^2+2(-a_7k_7+k_7+(a_9-1)k_9)dy_G-(a_3-1)(dy_G+1)^2k_3\\
&+(a_7-1)k_7-a_9k_9+k_9)dx_G+(a_3-1)(dy_G+1)^2k_3+(a_7-1)k_7+(a_9-1)k_9+dy_G(dy_G((a_4-1)k_4+(a_6-1)\\
&k_6+(a_7-1)k_7+(a_9-1)k_9)+2(-a_7k_7+k_7-a_9k_9+k_9)))+4d_{x,5}^3e_{**}n_{x,5}q_{2,5}-12d_{x,5}d_{y,5}^2e_{**}n_{x,5}q_{2,5}+d_{x,3}^4q_{1,3}\\
&-6d_{x,3}^2d_{y,3}^2q_{1,3}+d_{x,4}^4q_{1,4}-6d_{x,4}^2d_{y,4}^2q_{1,4}+d_{x,5}^4q_{1,5}-6d_{x,5}^2d_{y,5}(2e_{**}n_{y,5}q_{2,5}+d_{y,5}q_{1,5})+4e_{**}(d_{x,2}(n_{x,2}d_{x,2}^2-3d_{y,2}n_{y,2}d_{x,2}-3d_{y,2}^2n_{x,2})\\
&q_{2,2}+d_{x,3}(n_{x,3}d_{x,3}^2-3d_{y,3}n_{y,3}d_{x,3}-3d_{y,3}^2n_{x,3})q_{2,3}+d_{x,4}(n_{x,4}d_{x,4}^2-3d_{y,4}n_{y,4}d_{x,4}-3d_{y,4}^2n_{x,4})q_{2,4}))(\tilde{f}_G^{**})^{(0,2)}\\
&+4(d_{y,2}q_{1,2}d_{x,2}^3+e_*n_{y,2}q_{2,2}d_{x,2}^3+3d_{y,2}e_*n_{x,2}q_{2,2}d_{x,2}^2+a_1b_y(dx_G+1)^3(dy_G+1)k_1+a_2b_ydx_G{}^3(dy_G+1)k_2+b_y(a_3(dy_G+1)\\
&k_3(dx_G-1)^3+a_9(dy_G-1)k_9(dx_G-1)^3+a_4(dx_G+1)^3dy_Gk_4+a_5dx_G{}^3dy_Gk_5+a_6dx_G{}^3dy_Gk_6-3a_6dx_G{}^2dy_Gk_6-a_6dy_Gk_6\\
&+3a_6dx_Gdy_Gk_6-a_7dx_G{}^3k_7-3a_7dx_G{}^2k_7-a_7k_7-3a_7dx_Gk_7+a_7dx_G{}^3dy_Gk_7+3a_7dx_G{}^2dy_Gk_7+a_7dy_Gk_7+3a_7dx_Gdy_G\\
&k_7-a_8dx_G{}^3k_8+a_8dx_G{}^3dy_Gk_8)+3d_{x,5}^2d_{y,5}e_*n_{x,5}q_{2,5}+d_{x,5}^3e_*n_{y,5}q_{2,5}+d_{x,3}^3d_{y,3}q_{1,3}+d_{x,4}^3d_{y,4}q_{1,4}+d_{x,5}^3d_{y,5}q_{1,5}+3d_{x,3}^2d_{y,3}e_*n_{x,3}q_{2,3}\\
&+d_{x,3}^3e_*n_{y,3}q_{2,3}+d_{x,4}^2e_*(3d_{y,4}n_{x,4}+d_{x,4}n_{y,4})q_{2,4})(\tilde{f}_G^*)^{(1,1)}+4(-d_{y,2}q_{1,2}d_{x,2}^3+b_y((-(a_2-1)(dy_G+1)k_2-(a_3-1)(dy_G+1)\\
&k_3+(a_7-1)k_7+(a_8-1)k_8+(a_9-1)k_9+dy_G(-a_4k_4+k_4-a_5k_5+k_5-a_6k_6+k_6-a_7k_7+k_7-a_8k_8+k_8-a_9k_9+k_9))dx_G{}^3\\
&+3((a_3-1)(dy_G+1)k_3+(a_7-1)k_7-a_9k_9+k_9+dy_G(-a_4k_4+k_4+(a_6-1)k_6-a_7k_7+k_7+(a_9-1)k_9))dx_G{}^2\\
&+3(-(a_3-1)(dy_G+1)k_3+(a_7-1)k_7+(a_9-1)k_9+dy_G(-a_4k_4+k_4-a_6k_6+k_6-a_7k_7+k_7-a_9k_9+k_9))dx_G\\
&-(a_1-1)(dx_G+1)^3(dy_G+1)k_1+(a_3-1)k_3+(a_7-1)k_7-a_9k_9+k_9+dy_G((a_3-1)k_3-a_4k_4+k_4+(a_6-1)\\
&k_6-a_7k_7+k_7+(a_9-1)k_9))-3d_{x,5}^2d_{y,5}e_{**}n_{x,5}q_{2,5}-d_{x,3}^3d_{y,3}q_{1,3}-d_{x,4}^3d_{y,4}q_{1,4}-d_{x,5}^3(e_{**}n_{y,5}q_{2,5}+d_{y,5}q_{1,5})\\
&-e_{**}((3d_{y,2}n_{x,2}+d_{x,2}n_{y,2})q_{2,2}d_{x,2}^2+d_{x,3}^2(3d_{y,3}n_{x,3}+d_{x,3}n_{y,3})q_{2,3}+d_{x,4}^2(3d_{y,4}n_{x,4}+d_{x,4}n_{y,4})q_{2,4}))(\tilde{f}_G^{**})^{(1,1)}+(q_{1,2}d_{x,2}^4+a_1(dx_G+1)^4\\
&k_1+a_3k_3+a_4k_4+a_6k_6+a_7k_7+a_9k_9+dx_G(dx_G(6(a_3k_3+a_4k_4+a_6k_6+a_7k_7+a_9k_9)+dx_G\\
&(dx_G(a_2k_2+a_3k_3+a_4k_4+a_5k_5+a_6k_6+a_7k_7+a_8k_8+a_9k_9)-4(a_3k_3-a_4k_4+a_6k_6-a_7k_7+a_9k_9)))-4\\
&(a_3k_3-a_4k_4+a_6k_6-a_7k_7+a_9k_9)))+4d_{x,5}^3e_*n_{x,5}q_{2,5}+d_{x,3}^4q_{1,3}+d_{x,4}^4q_{1,4}+d_{x,5}^4q_{1,5}+4e_*\\
&(n_{x,2}q_{2,2}d_{x,2}^3+d_{x,3}^3n_{x,3}q_{2,3}+d_{x,4}^3n_{x,4}q_{2,4}))(\tilde{f}_G^*)^{(2,0)}+(-q_{1,2}d_{x,2}^4-(a_1-1)(dx_G+1)^4k_1-a_3k_3+k_3-a_4k_4\\
&+k_4-a_6k_6+k_6-a_7k_7+k_7-a_9k_9+k_9+dx_G((-a_2k_2+k_2-a_3k_3+k_3-a_4k_4+k_4-a_5k_5+k_5-a_6k_6\\
&+k_6-a_7k_7+k_7-a_8k_8+k_8-a_9k_9+k_9)dx_G{}^3+4((a_3-1)k_3-a_4k_4+k_4+(a_6-1)k_6-a_7k_7+k_7\\
&+(a_9-1)k_9)dx_G{}^2-6((a_3-1)k_3+(a_4-1)k_4+(a_6-1)k_6+(a_7-1)k_7+(a_9-1)k_9)dx_G+4((a_3-1)k_3-a_4k_4\\
&+k_4+(a_6-1)k_6-a_7k_7+k_7+(a_9-1)k_9))-4d_{x,5}^3e_{**}n_{x,5}q_{2,5}-d_{x,3}^4q_{1,3}-d_{x,4}^4q_{1,4}-d_{x,5}^4q_{1,5}\\
&-4e_{**}(n_{x,2}q_{2,2}d_{x,2}^3+d_{x,3}^3n_{x,3}q_{2,3}+d_{x,4}^3n_{x,4}q_{2,4}))(\tilde{f}_G^{**})^{(2,0)})\mathbf{h}^4
\end{aligned}
$$

With $\left(\tilde{f}_G^*\right)^{(i,j)}=\frac{\partial^{i+j}f_G^*}{e_*\partial x^i\partial y^j}$ and $\left(\tilde{f}_G^{**}\right)^{(i,j)}=\frac{\partial^{i+j}f_G^{**}}{e_{**}\partial x^i\partial y^j}$.

Corresponding author
Alexander Idesman can be contacted at: alexander.idesman@ttu.edu